Cohesin is essential for the timely activation of condensin and anaphase segregation

Jonay Garcia-Luis[1], Hélène Bordelet[2], Agnès Thierry[2], Romain Koszul[2,*] & Luis Aragon[1,*]

[1]DNA Motors Group, MRC London Institute of Medical Sciences (LMS), Du Cane Road, London W12 0NN, United Kingdom

[2]Régulation spatiale des génomes, Institut Pasteur, CNRS UMR3525, 75015 Paris, France

* Corresponding authors. luis.aragon@lms.mrc.ac.uk; romain.koszul@pasteur.fr

Abstract

Chromosome segregation requires the separation of sister chromatids and the sustained condensation of chromatids during anaphase. Yeast cohesin has a dual function on metaphase chromosomes, holding sister chromatids together and organising individual chromatids into loops. Cleavage by separase is thought to remove all cohesin from chromosomes at the anaphase onset. This fulfils the requirement for chromatid separation, but it is unclear how the structure of segregating chromatids is maintained following cleavage. Here we demonstrate that auxin-mediated degradation of cohesin's kleisin in anaphase, causes catastrophic chromosome mis-segregation demonstrating that cohesin affects post-metaphase processes. We identify a pool of cohesin bound to anaphase/telophase chromosomes and demonstrate that its inactivation causes defects in the organisation of centromeric regions and condensin function. Our data thus uncovers an unsuspected role for cohesin on anaphase/telophase chromosomes that is essential for the fidelity of segregation.

One sentence summary: Cohesin complexes on segregating chromosomes provide centromere structure and regulate condensin activity, demonstrating that cohesin has active roles after metaphase.

Introduction

Mitotic chromosome condensation solves two structural problems during chromosome segregation: firstly, it eliminates entanglements between replicated chromatids, and secondly, it compacts chromosomes so that they avoid being cut by the cytokinetic furrow at the end of mitosis [1]. From this, it follows that chromosome compaction must be maintained during anaphase segregation as sister chromatids are pulled towards opposite spindle poles.

Cohesin complexes were first proposed to impact on chromosome architecture by both providing cohesion between sister chromatids [2, 3] and promoting chromosome condensation during mitosis [2]. Cohesin's role in sister chromatid cohesion has dominated research in the cohesin field for over a decade [4]. The discoveries that (i) separase cleaves cohesin's kleisin Mcd1/Rad21/Scc1 subunit (hereafter referred to as Mcd1) at anaphase onset to trigger chromosome segregation, [5, 6] and that (ii), the N-end rule pathway rapidly degrades cleaved Mcd1 fragments [7] suggested that cohesin has no functions during anaphase and telophase.

Recent work has revived the original observation that cohesin serves a structural function on chromosomes [2] by demonstrating that cohesin plays a critical role in interphase and metaphase chromosome organisation. Chromosome capture (Hi-C) techniques have revealed that cohesin mediates intrachromosomal loops that are responsible for compacting mitotic chromosome arms, independently of cohesin's role in sister chromatid cohesion [8-10]. In contrast to yeast, mammalian cohesin organises chromosomes into loops during interphase [11] and dissociates from chromosome arms during prophase [12]. At metaphase mammalian cohesin is retained at centromeres where it provides cohesion [12], while the related SMC complex, condensin, takes over the role of folding chromosome arms into loops [13].

In yeast, condensin is also involved in chromosome condensation [14] but its function is mainly focused on the ribosomal gene array [8, 9]. Like cohesin [15, 16], condensin is also capable of extruding DNA loops [17, 18], an activity that is at the core of their structural roles in genome folding. Higher eukaryotes have two distinct condensin complexes, condensin I and II [19]. In mitosis, condensin II organises large (200- to 400-kb) loops,

while condensin I sub-divides these into smaller loops (80-kb)[13]. In contrast, yeast cells have a single condensin complex [14], with a structural function in metaphase chromosomes that is focused on specific genomic regions, including the ribosomal DNA array [9]. In yeast, the activity of condensin is heavily influenced by phosphorylation. Cyclin-dependent kinases (CDK), Polo and Aurora kinases have been shown to contribute to the fine-tuning of condensin activity in mitosis [20-23]. Condensin is relocalised from centromeres to chromosome arm regions as cells undergo segregation [24] thus promoting the separation of sister chromatids as it displaces cohesin complexes from chromosome arms [25]. Therefore, a coordination of the activities of cohesin and condensin complexes seems to be important as sister chromatids are segregated away from each other during anaphase. Consistent with this possibility, it has been recently demonstrated that Polo kinase bound to cohesin complexes promotes phosphorylation of condensin and that this is critical to ensure the structure of the ribosomal gene cluster (*RDN*) in metaphase [8, 26].

Here we have studied the effect of removing cohesin function in cells transiting through anaphase. We have used two complementary approaches, TEV-mediated cleavage and auxin-mediated degradation of cohesin's kleisin, Mcd1. We show that while TEV-mediated cleavage allows for bulk nuclear segregation, Mcd1 degradation results in the complete failure of chromosome segregation. We demonstrate that a population of cohesin complexes are present on segregating chromatids during anaphase/telophase and show that they are important for centromere organisation. Moreover, we find that the presence of this anaphase cohesin pool has an effect on condensin phosphorylation and activity. Together, these findings reveal that cohesin has essential roles post-metaphase.

Results

Cleavage of cohesin's kleisin causes bulk nuclear segregation

To study the role of cohesin on chromosomes after the loss of sister chromatid cohesion, we revisited some of the early experiments that investigated cohesin removal from chromosomes at the anaphase onset. The finding that engineered Mcd1 cleavage in metaphase, using TEV (tobacco etch virus) protease expression and TEV recognition sites in Mcd1 (Fig. 1a), triggered sister chromatid separation [6] provided a strong

argument in favour of the idea that the main function of cohesin in chromosome segregation is to hold sister chromatids together prior to their separation. Based on these findings it has been widely assumed that the function of cohesin is finished after metaphase. It is important to note that TEV-mediated anaphase experiments are technically complex because they require blocking cells in metaphase for extended periods of time [6]. The metaphase arrest employed was mediated by depletion of Cdc20 (an activator of the anaphase-promoting complex, APC) using the methionine promoter, which is relatively unstable. We therefore decided to re-evaluate chromosome segregation in TEV-mediated anaphases using the original strains (Fig. 1a) as well as newly developed ones (Fig. 2). In brief, an engineered version of Mcd1 where the TEV cleavage recognition site 'ENLYFQ*G' substituted the second endogenous separase recognition site 262'SVEQGR*R'269 [6] was used (Fig. 1a). Cells carried the TEV protease under the inducible *GAL* promoter and a copy of the *CDC20* gene under the *MET3* promoter to induce metaphase arrest [6]. Induction of TEV expression on Cdc20-arrested cells led to cleavage of Mcd1 after 60 min (Fig. 1a). However, bulk nuclear segregation was not observed until 90-120min following the induction (Fig 1b). Chromosome tags at *CEN5* showed that separation of centromere-proximal regions occurred efficiently in TEV-induced anaphase (Fig. 1c, 1d). However, nuclear staining revealed anaphase bridges connecting the separated nuclei in a subset of cells (Fig. 1c) indicating that full segregation of the genome had not been achieved. To further investigate this, we introduced a second chromosome tag in the distal region of chromosome 4 (*TEL4*) (Fig. 1d), since telomeric regions of large chromosomes are more challenging to segregate than centromeres. We observed that *TEL4* tags did not segregate correctly in a subpopulation of cells (Fig. 1d). This result demonstrates that while bulk nuclear segregation is achieved in TEV-mediated anaphases, correct segregation of all chromosomes, particularly larger ones, is not.

Previous studies had suggested that in TEV-triggered anaphases, the Cdc14 mitotic exit phosphatase is not fully activated [27] thus generating microtubule instability [28] which potentially could impair the movement of chromosomes to cell poles [28]. This was used as an argument to explain, at least in part, why TEV-induced anaphases, similarly to *cdc14* conditional mutants, cannot segregate telomeric regions of long chromosomes efficiently [28, 29]. We noticed that in TEV anaphases the cleaved C-terminal fragment of Mcd1 is fully stable (Fig. 1a). In contrast, Mcd1 cleavage by separase produces a C-

terminal fragment that is rapidly degraded by the N-end rule pathway [7]. The lack of Mcd1 fragment degradation after TEV-induced cleavage stems from the fact that TEV protease cleavage occurs following the glutamine (Q) residue of the TEV recognition site ('ENLYFQ*G') leaving a glycine (G) as the N-terminal residue (referred to as TEVG), which is not well recognised by the N-rule pathway [30]. In contrast, separase cleavage leaves an arginine (R) residue at the N-terminus of the cleaved product ('SVEQGR*R'), which is a good substrate for N-end rule degradation [30]. Interestingly, Beckouet *et al* [31] have shown that following TEV-induced cleavage both the C-terminal and N-terminal fragments of Mcd1 are stabilised. Therefore, we considered the possibility that failure to rapidly degrade the residual Mcd1 products after TEV cleavage might contribute to the defective segregation of large chromosomes and hence the phenotypes observed (Fig. 1d). To test this idea, we first investigated whether Mcd1 fragments remain associated with the Smc core subunits of cohesin after TEV-induced cleavage. We introduced FLAG and HA tags at the N- and C-termini of Mcd1, respectively, to detect the two products generated by TEV cleavage (Fig. 2a). We also tagged Smc3 with the V5 epitope to investigate the presence of Mcd1 fragments in Smc3 immunoprecipitates performed at different times during TEV-induced cleavage (Fig. 2a). We observed that both N- and C-terminal Mcd1 fragments remain associated to Smc3 after TEV cleavage of Mcd1 (Fig. 2a, S1a). This, though surprising, supports the possibility that complete cohesin rings (albeit cleaved at Mcd1) might hinder the segregation of long chromosomes in TEV-induced anaphases.

To further test this possibility, we decided to use a TEV recognition site on Mcd1 that was able to yield a Mcd1 C-terminal fragment with a terminal amino-acid recognized by the N-end rule pathway. We found this to be the case when we used the TEV recognition site 'ENLYFQ*F' (referred to as TEVF) (Fig. 2b). This site leaves a phenylalanine, rather than a glycine, as the N-terminal aminoacid after TEV cleavage. Importantly, N-terminal phenylalanine is a good substrate for N-end rule degradation [30]. Mcd1 was cleaved in both TEVF and TEVG sites with similar kinetics (Fig. 2b-c). As previously reported [31] both cleavage fragments were stable for long periods when TEV cleaved at TEVG recognition sites (Fig. 2c). In contrast, both N- and C-terminal fragments were rapidly degraded after TEV cleavage on TEVF sites (Fig. 2b). Next, we compared the segregation kinetics of chromosome tags located on the centromere distal parts of chromosome 4 and 5 (Fig. 2d, S1b) in cells carrying the different TEV

recognition sites in Mcd1. Bulk nuclear segregation in TEV-induced anaphases was similar in cells carrying Mcd1 alleles with both recognition sites (Fig. 2b-c, 2d). However, we detected an increase in the level of chromosome mis-segregation for both chromosomes 4 and 5 in cells carrying TEVF recognition sites (Fig. 2d, S1b) compared to those with TEVG sites. This result was surprising since we expected that full fragment degradation in TEVF-induced anaphases would improve the segregation defects observed in cells carrying the canonical TEV recognition site, TEVG.

Auxin-mediated degradation of Mcd1 causes acute chromosome missegregation

The higher level of chromosome mis-segregation observed in TEV-induced anaphases in cells carrying the TEVF recognition site (Fig. 2b) was puzzling given that, as predicted from the literature [6], Mcd1 should be dispensable after cells achieve bipolar attachment to the spindles because cohesin is not anticipated to play any role during anaphase/telophase. The difference in mis-segregation between cells cleaved by TEV when using TEVG and TEVF recognition sites lies in the degradation of the two cleavage products (Fig. 2b-c), suggesting that, although counterintuitive, increased degradation of Mcd1 fragments worsens segregation (Fig. 2d). We also observed that a small amount of full-length Mcd1 resisted TEV cleavage (Fig. 2b-c), raising the possibility that TEV only removes a subset of cohesin complexes.

To further explore these possibilities, we searched for an alternative approach to induce the rapid removal of Mcd1. To this aim, we used an auxin-inducible degron allele of Mcd1 (*MCD1-AID*) [32] which allows rapid degradation by poly-ubiquitylation upon exposure to auxin (Fig. 3a). Cells carrying Mcd1-AID were arrested in metaphase by depletion of Cdc20 and then exposed to auxin (Fig. 3a). Degradation of Mcd1 occurred rapidly and was completed within 30-60min (Fig. 3a-d). Therefore, the Mcd1-AID allele provided us with a powerful tool to rapidly eliminate Mcd1.

Auxin-mediated degradation of Mcd1 in Cdc20 arrests caused cells to enter pseudo-anaphases (Fig. 3b-c) where nuclei spent an unusually long time elongated (anaphase bridges) (Fig. 3b). We used two different chromosome tags, at arm and telomere regions, on chromosome 5 to analyse segregation (Fig. 3c). Chromosome mis-segregation was observed for both tags, with levels particularly high (>50%) for the telomere tag (Fig. 3c, Fig S2a-b). Chromosome tags inserted on the larger chromosome

4 confirmed the acute mis-segregation phenotype (Fig. 3d). Next, we compared chromatin binding stability of Mcd1 after cleavage or degradation in TEV and Mcd1-AID induced anaphases respectively. To this aim, we performed chromatin immunoprecipitation using Smc3 to test binding of this core cohesin subumit to various sites along chromosome 5. We calculated the amount of Smc3 relative to the metaphase block for each time point during anaphase. Smc3 binding was high across all sites 30 min post TEV induction and decreased at 60 min (Fig. 3e). In contrast, Smc3 binding was low in anaphases induced by auxin-mediated degradation of Mcd1 at early time points (<10% at 30 min) (Fig. 3e). These results confirm that TEV cleavage is slower while degradation in Mcd1-AID is faster and removes the majority of bound cohesin.

Importantly, the slower kinetics of TEV-mediated cleavage correlate with the removal of cohesive complexes, indicated by the better separation of sister chromatids achieved in these cells (Fig. 2b-d). On the other hand, the faster degradation of Mcd1 using the auxin approach removes most complexes, both, cohesive and loop extruding (structural) cohesin, thus preventing any potential functions in anaphase which could explain the catastrophic segregation observed (Fig. 3c-d). These results demonstrate that cohesin has a role, or at least a direct effect during anaphase, required for sister chromatids to segregate correctly independently of its role in sister chromatid cohesion.

Chromosome organisation is lost in the absence of cohesin

In addition to sister chromatid cohesion, cohesin mediates intrachromosomal loops in metaphase arrested chromosomes, providing a structural framework for the compaction of chromosome arms [8, 9]. How chromosomes are organised during anaphase, when individual chromatids are being pulled to the poles, is not well understood. While yeast metaphase chromosomes rely on cohesin for *cis* looping and arm organisation, it is not known how they maintain arm structure once separase has cleaved cohesin. In our TEV- and auxin-induced anaphases, cells are first arrested in metaphase using depletion of Cdc20. Therefore, cleavage or degradation of Mcd1 in these experiments is likely to affect the organisation of chromosome arms. To test this, we built Hi-C libraries from cells where either Mcd1 had been cleaved by TEV or had been degraded using the Mcd1-AID allele. To build these libraries, we used timepoints when the bulk of Mcd1 had been either cleaved or degraded depending on the experiment (Fig. 4a). This was 90 min after cleavage for TEV-induced anaphases, and 60 min after auxin addition for

Mcd1-AID mediated anaphases (Fig. 4a). Following sequencing, we computed the corresponding normalised genome-wide contact maps for Mcd1-TEVG and Mcd1-AID anaphases (Fig. 4b). When we compared the contact maps of individual chromosomes obtained from cells arrested in metaphase using Cdc20 depletion (Fig. 4b), to those obtained for Mcd1-TEVG and Mcd1-AID, we observed a significant decrease in intrachromosomal contacts in both experimental conditions (Fig. 4b-c, S3a). The contact probability (P) as a function of genomic distances of all chromosome arms showed a reduction of contacts in the 10-30kb range for Mcd1-TEVG and Mcd1-AID samples compared to Cdc20 arrests (Fig. 4c, S3a). Notably, the reduction in Mcd1-AID was more pronounced than in Mcd1-TEVG (Fig. 4c). These results show that chromosome arm structure is disrupted, particularly in Mcd1-AID cells, and that the acute removal of cohesin not only removes cohesion but also causes the collapse of chromosome structure, which explains why orderly chromosome segregation cannot be achieved (Fig. 3). This raises two important questions; (i), are all cohesin complexes removed from chromosomes at anaphase onset, and (ii) how is the cohesin-dependent organisation of chromosomes maintained during anaphase following separase cleavage? We sought to explore these possibilities.

Cohesin is present on telophase chromosomes and its inactivation causes structural defects on rDNA and centromeres

Previous studies have reported the presence of cohesin on chromosomes during anaphase [25], however these studies concluded that such complexes were residual proteins that had escape cleavage and carried no function. We decided to investigate whether cohesin complexes are retained on chromatin during the anaphase and telophase stages of mitosis and whether they carry out any function.

First, we evaluated the levels of full-length Mcd1 present in telophase as a proxy for the quantity of cohesin complexes that escape separase cleavage. To this aim, we followed full-length Mcd1 in a cell culture undergoing highly synchronous cell division. To ensure the highest degree of synchronicity we used a combination of cell cycle blocks and conditional mutant alleles. The culture was first arrested in G_1 using the mating pheromone α-factor, before being released to a nocodazole-mediated metaphase block (Fig. 4d). From the nocodazole arrest, cells were allowed to proceed

into anaphase but blocked at telophase using the *cdc15-2* allele [33]. Finally, telophase arrested cells were released into the next G_1 (Fig. 4d). Samples were taken every 10-20min and the levels of Mcd1 were followed by Western blotting (Fig. 4d). As expected, a significant drop in the levels of full-length Mcd1, accompanied by the appearance of Mcd1 cleavage, were detected upon anaphase entry (Fig. 4d). Surprisingly, we observed some recovery of Mcd1 full-length levels while cells were arrested in telophase (Fig. 4d). This prompted us to further investigate whether cohesin complexes are present on telophase chromosomes. To this aim, we first fused the green fluorescent protein (GFP) to cohesin subunit Smc3 and imaged its localisation on telophase arrested cells (Fig. 4e). Smc3-GFP signal was observed on segregated nuclei, with a clear discrete dot present at the cell poles that colocalised with the spindle pole body protein Spc29 (Spc29-RedStar2) (Fig. 4e). This suggests that Smc3-GFP signal is indeed enriched at the centromeric regions of telophase chromosomes. Cohesin plays an active role in the compaction of the ribosomal gene array (rDNA) on chromosome XII during metaphase [21]. We therefore tested whether inactivation of cohesin in telophase arrested cells causes compaction defects on rDNA. To this aim, we used an analogue-sensitive allele (AS) of *cdc15-as* and the temperature sensitive allele of *mcd1-73*. We also expressed *NET1*-yeGFP in these cells to evaluate the compaction of rDNA. Inactivation of cohesin in the arrests caused decondensation of rDNA signals (Fig. 4f), demonstrating that cohesin plays an active role compacting rDNA in this late mitotic stage.

Next, we sought to detect the amount of cohesin bound to chromosomes in *cdc15*-arrested cells using Mcd1-6HA and calibrated ChIP-seq. To identify the normal position of cohesin binding sites along chromosomes, we used Smc1 localisation on metaphase arrests (Fig. 4g, S3b). We subtracted the background signal from our experiments using untagged cells arrested either on metaphase (nocodazole) or *cdc15*-2 (Fig. 4g). The number of cohesin binding sites per chromosome was significantly reduced in telophase arrested cells, however, discrete arm sites were observed on some chromosomes and, importantly, enrichment at centromere regions was evident (Fig. 4g).

Next, we decided to test whether cohesin bound to telophase chromosomes plays any structural role. To do this, we arrested cells in telophase using an analogue-sensitive

allele of Cdc15. In addition to *cdc15-as*, we inactivated cohesin using the Mcd1-AID and Smc3-AID alleles (Fig. S3b). We build Hi-C libraries from cells arrested in telophase, where Mcd1 had been degraded (*cdc15-as* Mcd1-AID) after the arrest. To ensure complete cohesin removal, we also generated libraries from *cdc15-as* cells where both Mcd1 and Smc3 had been degraded upon telophase arrest (Fig. 4h, S3c). Comparison of the contact maps revealed changes at centromeric regions in telophase cells depleted for cohesin (Fig. 4h). This finding is in agreement with our ChIP-seq and cytological analysis demonstrating that cohesin is bound to these regions (Fig. 4e). Degradation of cohesin led to decreased isolation of *CEN*-proximal regions from other sites down chromosome arms *in cis* (Fig. 4i), demonstrating that cohesin complexes influence intrachromatid contacts at centromeres in telophase chromosomes. In addition, the *in trans* interaction of *CEN* sequences was reduced in *cdc15-as* cells with depleted cohesin (Fig. 4j). This shows that cohesin degradation also affects clustering of centromeres between different chromosomes. These results confirm that cohesin is present at centromeric sites on telophase chromosomes where it influences their structure.

Cohesin presence impacts on condensin phosphorylation levels

Recent studies have shown that cohesin indirectly affects the phosphorylation of condensin promoting compaction of the ribosomal gene cluster (*RDN*) on chromosome XII in metaphase cells [26]. Cohesin is phosphorylated during mitosis by several kinases, including Polo kinase Cdc5 [34]. Phosphorylation of Mcd1 by Cdc5 enhances the rate of separase cleavage both *in vitro* and *in vivo* [34]. Importantly, Cdc5 directly associates with chromatin-bound cohesin through Mcd1's Polo binding domain (PBD) [35]. Condensin is also a target of Polo kinase [22] and its phosphorylation enhances condensin's overwinding activity [22] as well as being necessary for its relocalisation from centromeres to chromosome arms [24]. We considered that cohesin might also influence the activity of condensin function at genomic regions other than rDNA and thus, cohesin degradation in anaphase could not only disrupt centromere structure but also lead to a general deregulation of condensin activity.

To further explore this we evaluated the phosphorylation status of condensin's subunit Ycg1 in a synchronised cell cycle in the presence and absence of cohesin (Fig. 5a). We released cells from a G_1 block into a metaphase block induced by Cdc20 depletion. In

wildtype cells, Ycg1 phosphorylation was observed as cells accumulated in metaphase (Fig. 5a), as expected [22]. Condensin phosphorylation was also observed when Mcd1 was degraded in released cells (Fig. 5a). However, phosphorylation was significantly higher in cells lacking Mcd1 (Fig. 5a) indicating that the presence of cohesin in metaphase prevents hyper-phosphorylation of the condensin subunit Ycg1 (Fig. 5a). In addition, condensin phosphorylation negatively correlated with the presence of Mcd1 in cells released from metaphase into a new cycle (Fig. 5b). Ycg1 phosphorylation increased as cells were released from nocodazole, when Mcd1 is cleaved, and sharply decreased as Mcd1 accumulated in the subsequent G2/M phase (Fig. 5b). Moreover, degradation of Mcd1 while cells were arrested in metaphase led to an increase in Ycg1 phosphorylation (Fig. 5c). Degradation of Polo kinase in metaphase arrested cells caused a significant reduction in Ycg1 phosphorylation (Fig. 5d), therefore, as expected, Ycg1 phosphorylation largely depended on Polo kinase Cdc5.

Finally, we tested phosphorylation of Ycg1 in a mutant allele of Mcd1 where Cdc5 binding is impaired due to the removal of Cdk1 priming phosphorylation sites (Mcd1-15A) [35] (Fig. 5e). We released Mcd1-15A cells from G_1 and evaluated the levels of Ycg1 phosphorylation during the synchronised cycle (Fig. 5f). Ycg1 phosphorylation was increased in Mcd1-15A cells compared to wildtype cells (Fig. 5f) confirming that condensin hyperphosphorylation is a direct consequence of the decreased interaction between Cdc5 polo kinase and cohesin. Together, these results suggest that Cdc5 phosphorylation of Ycg1 is inhibited and subsequently regulated by normal levels of cohesin on chromosomes.

Premature condensin hyper-phosphorylation causes segregation defects

Abrupt cohesin degradation in metaphase arrested cells leads to depletion of chromosome structuration and has a negative impact in the ability of cells to segregate chromosomes correctly (Fig. 3c-d). Abrupt cohesin degradation also causes premature hyper-phosphorylation of condensin (Fig. 5c). We sought to investigate whether premature condensin hyper-phosphorylation is also implicated in the chromosome segregation defect observed when cohesin is acutely removed. We first tested whether an increase in the pool of cellular Cdc5 kinase impacted chromosome segregation. Expression of Polo kinase from the strong *GAL1-10* promoter causes an increase in

Ycg1 phosphorylation [22] (Fig. 6a). We therefore used this approach to investigate its effect on chromosome segregation.

To this aim, we blocked cells in metaphase and overexpressed Cdc5 before releasing cells into anaphase (Fig. 6b). To score segregation we ensured that cells did not exit mitosis by blocking them in telophase (Fig. 6b) using an auxin degron on Cdc15 (*CDC15-AID*). In the absence of Cdc15, cells are able to segregate chromosomes but cannot exit telophase [33]. Cells exposed to galactose, with Cdc5 overexpressed, experienced difficulties during segregation, as evidenced by the increased levels of anaphase bridges and mis-segregation (Fig. 6b). We also used tags to measure the distances between separated chromosomes in the telophase arrests as a proxy for the efficiency of segregation (Fig. 6c). Cells with higher levels of Cdc5 exhibited shorter distances between chromosome tags indicating that they had more difficulties during segregation.

While these results suggest that higher Ycg1 phosphorylation might reduce segregation efficiency, an increased pool of Polo kinase could also impact segregation through other mitotic targets [36]. To rule out this possibility, we decided to employ a more direct approach to specifically increase Cdc5 phosphorylation of condensin. To achive this, we used Cre-mediated recombination to generate a fusion protein between condensin's subunit Brn1 and Cdc5 Polo kinase (Fig. 7a, Fig S4). As a control, we fused Brn1 to a kinase-dead version of Cdc5 (Cdc5-KD) (Fig. 7a). Cells carrying the Brn1-Cdc5 fusion exhibited mild growth defects (Fig.7a-b) while cells with the Brn1-Cdc5KD fusion showed wildtype levels of growth (Fig.7a). Importantly, we observed Brn1 and Ycg1 hyper-phosphorylation in cells carrying the Brn1-Cdc5 fusion compared to Brn1-Cdc5KD control cells (Fig. 7b, S4) confirming that our experimental strategy had caused an increase in phosphorylation of condensin. Next, we studied the effect of Brn1-Cdc5 fusion on chromosome segregation. We used a strain carrying an auxin-degron in Cdc15 to ensure telophase arrests to facilitate the study of segregation of chromosome tags (Fig. 7c-d). Cells were blocked in G_1 and released in the presence of auxin to ensure degradation of Cdc15. We compared segregation of tags in cells carrying the Brn1-Cdc5 or Brn1-Cdc5KD fusions (Fig. 7c-d). Cells expressing Brn1-Cdc5 exhited greater difficulties during segregation, having an accumulation of cells arrested in anaphase (35%) and increased tag missegregation (20%) (Fig. 7c). When

we measured the distance between chromosome tags we found shorter distances in cells expresing Brn1-Cdc5 compared to Brn1-Cdc5KD, indicating that these cells experience more difficuulties during chromosome segregation (Fig. 7d). To further confirm that expression of Brn1-Cdc5 led to the observed chromosome missegregation, we compared the rate of plasmid loss in Brn1-Cdc5 and Brn1-Cdc5-KD using centromeric plasmids habouring the *ADE2* marker (Fig. 7e). Loss of the *ADE2* gene leads to change in colony colour from white (*ADE2+*) to red (*ade2-*) and this can be used to infer plasmid loss. A significant increase in plasmid loss was observed in Brn1-Cdc5 cells grown in full media compared to Brn1-Cdc5-KD cells (Fig. 7e), thus confirming plasmid missegregation. This phenotype was further increased when cells were forced to divide faster at 37°C (Fig. 7e). Next we sought to determine if the defect in condensin fuction during chromosome segregation in the cells harbouring the fusion Brn1-Cdc5 could also be observed at the rDNA locus (Fig. 7f). Condensin activity and its phosphorylation status govern the structure of the rDNA array during mitosis [1, 14, 22], and cells harbouring phosphomutants of condensin exhibit a defective structure of the rDNA [22]. We used a strain carrying either Brn1-Cdc5 or Brn1-Cdc5KD, an auxin degron in Cdc16 (*CDC16-AID*) to arrest the cells in metaphase, and Net1 tagged with GFP (NET1-yeGFP) to visualise the rDNA in these cells. To have a quantitative measure of the rDNA shape we measured the length of the Net1-GFP signal. This showed that hyper-phosphorylation of condensin has a dramatic impact on the structure of the rDNA. We observed an rDNA length of 0.5 μm for the Brn1-Cdc5 fusion compared to 2 μm in Brn1-Cdc5KD (Fig. 7f).

Hi-C studies have revealed that condensin contribution to metaphase compaction along chromosome arms is limited to the rDNA proximal regions of the right arm of chromosome XII [9]. In addition to this, condensin removal causes decreased association between centromeres in *trans* as well as increased isolation between centromeric regions and chromosome arms in *cis* [9]. We decided to investigate the effect of Brn1 hyper-phosphorylation on both, the organisation of centromeric regions and the compaction of chromosome XII arms. To this aim, we generated Hi-C libraries from cells arrested in metaphase expressing either the Brn1-Cdc5 or the Brn1-Cdc5-KD fusions (Fig. 8a). As expected, we did not observe global changes in chromosome organisation when we compared Brn1-Cdc5 and the Brn1-Cdc5-KD fusion maps or

contact probability as a function of the genomic distance (Fig. 8a, S5a). However, analysis of individual centromeres revealed increased isolation of *CEN* regions from chromosome arms in *cis* for Brn1-Cdc5 compared to Brn1-Cdc5-KD (Fig. 8b). In contrast, we observed no changes between centromeres *in trans* (Fig. 8c). Next, we looked at the rDNA proximal region of the right arm of chromosome XII. Brn1-Cdc5 maps showed a reduction in interactions (Fig. 8d), demonstrating that hyperphosphorylation of condensin causes structural defects for this region (Fig. 8d). This defect was also evident when we plotted the contact probability (P) as a function of genomic distance (s) for the rDNA proximal region (Fig. 8e) thus reproducing the trend observed when condensin is depleted in metaphase [9].

Collectively our analysis of the Brn-Cdc5 fusion reveals that untimely hyper-phosphorylation of condensin, causes defects in chromosomes structure similar to those reported for condensin inactivation, as well as errors in chromosome segregation. Therefore, we conclude that in addition to its structural role during anaphase/telophase, the effect that cohesin levels have on condensin phosphorylation have a direct consequence on its activity. These results demonstrate that cohesin binding to Cdc5 acts as a temporal fine-tunning switch for the activation/function of condensin.

Discussion

The role of cohesin complexes in supporting mitotic chromosome architecture has long been established [2, 3], however, while their prominent role in mediating sister chromatid cohesion has been intensively studied, their contribution to chromosome folding has only recently become topical with the advent of Hi-C techniques [37, 38]. Here we set out to explore whether cohesin influences or plays a role in chromosome structuration and segregation after the anaphase onset.

Cohesin is loaded onto chromosomes by the loader complex Scc2/4 [39] during G_1 and becomes cohesive during DNA replication [40]. The cohesive state requires the acetylation of cohesin Smc3 by the Eco1 acetyl-transferase to make cohesin refractory to an inhibitory “anti-establishment” activity dependent on Wapl [41, 42]. In yeast, the removal of cohesin from chromosomes at the anaphase onset involves the cleavage of one of cohesin subunits, Mcd1/Scc1 by the protease separase (Esp1) [5, 6]. Separase

function is highly regulated to prevent its premature activation before every single chromosome has been aligned on the mitotic spindle. Firstly, separase activity is blocked by a bound inhibitor named securin (Pds1) [39], which is destroyed by ubiquitin-mediated proteolysis once cells are ready to enter anaphase [43]. Secondly, separase-mediated cleavage of Mcd1 is primed by Polo-kinase (Cdc5) dependent phosphorylation of Mcd1 at serines 175 (S175) and 268 (S268), within the cleavage site [34]. This double regulation ensures that cohesion is not destroyed before it should be. However, once separase is activated at the anaphase onset, cohesin is thought to be abruptly and completely removed from yeast chromosomes [4]. In contrast to yeast, in metazoans and vertebrates cohesion is maintained throughout G_2, and at the onset of mitosis, loosening of arm cohesion and removal of cohesin accompanies the compaction of each chromatid along its longitudinal axis [44]. Early studies on the role of cohesin during mitosis concluded that this SMC complex is important for the bipolar attachment of chromosomes [45] and did not attribute any roles after separase cleavage [4]. These studies employed TEV-mediated cleavage of Mcd1 in metaphase arrested cells to trigger chromosome separation and concluded that cohesin cleavage triggered full chromosome segregation [6]. We revisited this and found that in agreement with the original study, TEV-mediated cleavage of cohesin, precipitates bulk nuclear segregation, despite the fact that not all chromosomes segregate correctly (Fig 1c-d).

We noticed that TEV-mediated cleavage was slow and did not remove all cohesin from chromosomes (Fig. 2b-c). We hypothesised that a more efficient method to remove cohesin complexes might prevent the minor segregation defects observed. Surprisingly, these improved methods, including variants of TEV recognition (TEVF) and auxin-mediated degradation did not improve segregation but instead caused catastrophic anaphases where many cells became arrested with anaphase bridges and unseparated nuclear masses (Fig.3b-d). This unexpected result suggested that cohesin might be important post-metaphase (i.e. after separase cleavage) and triggered us to explore the reasons behind this penetrant phenotype. First, we observed that removing cohesin in metaphase arrested cells, leads to a collapsed organisation of chromosome arms (Fig. 4a-b). Hi-C analyses showed that Mcd1 degradation caused defects in the 10-30kb range of *cis* interactions that are characteristic of cohesin-dependent loops (Fig. 4b-c). Therefore, despite removal of sister chromatid cohesion, the loss of structure of chromosomes during anaphase, particularly when Mcd1 is degraded by auxin, likely

prevented segregation. Importantly, the phenotypes observed when cohesin function was disrupted with TEV-induced cleavage or auxin-mediated degradation were clearly distinct. In TEV anaphases we observed almost complete nuclear separation (Fig. 1b), in contrast, segregation was severely disrupted when Mcd1 was degraded using the auxin system (Fig. 3b-d). Hi-C analysis showed that the disruption in the 10-30kb range of *cis* contacts was greater when Mcd1 was degraded rather than cleaved by TEV (Fig. 4c). These results suggest that TEV cleavage targets cohesive cohesin well but it is less efficient in removing complexes involved in the organisation of chromosome loops (i.e. loop extruding complexes). In contrast, auxin-mediated degradation of Mcd1 seems to equally disrupt cohesin complexes engaged in both cohesion and loop extrusion functions. We observed that upon TEV cleavage, Mcd1 fragments still interact with the Smc subunits (Fig. 2a). A mechanistic difference between cohesive cohesin and loop extruding complexes lies in the way that these complexes interact with the DNA substrate. While cohesive cohesin topologically embraces DNA [46], loop extruding complexes rely on non-topological interactions [15]. It is likely that cohesin complexes cleaved by TEV are still able to interact non-topologically with the DNA substrate and can perform loop extrusion, thus explaining why TEV-cleavage has only a modest effect on the structural role of cohesin, while completely disrupting the cohesive role (that depends on topological association).

Based on evidence that suggested a role for cohesin post-metaphase (Fig. 3c-d, 4b-c) we sought to test the presence of cohesin on chromosomes arrested in telophase. Although a large proportion of cohesin complexes are removed from chromosomes by separase (Fig. 4d, g), we detected binding of cohesin to several genomic regions on chromosomes at telophase (Fig. 4g). In particular, centromeres showed clear enrichment of cohesin during this late mitotic stage (Fig. 4g). Depletion of cohesin subunits in telophase revealed that bound cohesin during this late mitotic stage is still influencing the structural organisation of pericentromeric regions, as well as promoting interactions between *CEN*-regions of different chromosomes (Fig. 4i-j). Moreover, we observed condensation defects at the ribosomal gene array on chromosome XII (Fig. 4f). Therefore, we conclude that cohesin is not completely removed from chromosomes at the anaphase onset as previously thought and instead a pool of chromatin-bound complexes organise specific chromosome regions (centromeres) until telophase. This

is consistent with the mis-segregation phenotypes observed in our cohesin depleted anaphase assays.

We also show that cohesin contributes to the temporal fine-tuning of condensin phosphorylation by Polo kinase Cdc5. Cdc5 is an important regulator of mitotic processes. Cdc5 is recruited to chromosomes by cohesin [35] but it also impacts on the function of condensin during mitosis because it phosphorylates three different condensin subunits during anaphase which results in the activation of condensin's supercoiling function [22]. This is important to ensure directionality of decatenation by Top2 and thus sister chromatid segregation [47, 48]. Recent work has uncovered a role for cohesin and Cdc5 in ensuring the establishment and maintenance of condensation of the 1-Mb long ribosomal DNA (*RDN*) [26]. Cdc5 is recruited to *RDN* by cohesin and promotes the downstream activation of adjacently bound condensin [26], which ensures appropriate rDNA compaction in metaphase. We have looked at how this crosstalk between cohesin and condensin affects the rest of the genome during chromosome segregation in anaphase. Consistent with previous findings [26], we observed that acute degradation of the cohesin subunit Mcd1 caused premature hyper-phosphorylation of condensin (Fig. 5). Importantly, it has been shown that Cdc5 binds to cohesin's Mcd1 subunit through its PBD [35]. We further confirm that Mcd1 binding to Cdc5 prevents premature hyper-phosphorylation of condensin by using a mutant Mcd1 allele (Mcd1-15A) that doesn't bind to Cdc5 (Fig. 5e-f). This mutant showed premature hyper-phosphorylation of condensin and caused chromosome segregation problems and genome instability. These results support the possibility that during the onset of anaphase the partial removal of cohesin by separase promotes a timely choreographed switch of Cdc5 activity from cohesin to condensin, carefully regulating its activity. Indeed, constitutive Cdc5-dependent hyper-phosphorylation of condensin forced when Brn1 is fused to Cdc5 leads to segregation defects (Fig. 7c-d). This is in agreement with previous reports showing that mis-regulation of condensin phosphorylation impairs its activity [49]. Furthermore, Hi-C analysis of Brn1-Cdc5 fusions exhibited defects consistent with defective condensin activity, including structural defects at centromere regions (Fig. 8b) and the region of the right arm of chromosome XII between the centromere and the ribosomal gene array (Fig. 8d-e) [9]. Collectively these results demonstrate that the timing of condensin activation, through Cdc5 phosphorylation, is

regulated by cohesin levels, and that this regulation is key to ensure timely chromosome structure and segregation.

During anaphase condensin relocalises from centromeres to telomeres facilitating chromosome condensation and decatenation by Top2 [24]. This translocation of condensin from centromeres to telomeres depends on polo kinase Cdc5, leading to higher binding rates for condensin and the promotion of its overwinding activity [24]. Earlier studies have shown that cohesin complexes are not removed from all chromosome sites at the anaphase onset, and instead residual cohesin was found to be present on *CEN*-distal chromosome sites and only removed by the coiling action of condensin during anaphase [25], as chromosome segregation proceeded from centromere to telomere regions. Together, these observations suggest a scenario where Cdc5 bound to cohesin might be important to regulate the timing of condensin activation along chromosome arms (Fig. 8f). It is possible that abrupt degradation of cohesin in our experiments (Mcd1-AID anaphases) leads to sudden disassembly of cohesin-mediated loops [8, 9] that together with the upregulation of condensin phosphorylation might generate a disordered substrate where hyperactivated condensin might not be able to direct successfully Top2 activity bias towards decatenation [47] and this further contributes to the segregation catastrophe observed.

Currently, cohesin functions during mitosis are thought to include; (i), the pairing of sister chromatids, (ii), the bipolar organisation of chromatids as they attach to the mitotic spindles and (iii), the organisation of metaphase chromosomes into looped domains. Recent work has shown that cohesin is necessary for the maintenance of the structure of the rDNA during metaphase and that this role is executed through the regulation of condensin localisation [26]. Importantly, these cohesin functions occur in metaphase cells and separase cleavage of cohesin at the anaphase onset has generated the perception that cohesin's roles are finished at the beginning of anaphase. Collectively our data demonstrates that cohesin removal from chromosome is not complete and abrupt. Instead, a progressive and fine-tuned cleavage of cohesin during anaphase/telophase is likely to allow the timely phosphorylation of condensin, indirectly contributing to the structuration and segregation of chromosomes at this stage. In addition, the binding of cohesin to centromeres detected in telophase arrested cells and the organisation defects observed in these regions when cohesin is depleted

in this cell cycle stage further demonstrate an active role for cohesin in these sites at late stages of mitosis. Therefore, these findings extend the repertoire of cohesin roles on chromosomes and demonstrate that this complex has important post-metaphase functions critical for ensuring faithful genome segregation.

Methods

Yeast strain

Yeast strains used in this study are listed in Table 1. Epitope tagging of genes was carried out as described in [50].

K9027	*MATα; MCD1Δ:HIS3; MCD1TEV268::LEU2; GAL-NLS-mcy9-TEVprotease-NLS2::TRP1 (*10-fold integrant by southern*); ura3::3xURA3 tetO112; his3::HIS3 tetR-GFP; MET3-HA3-CDC20::TRP1; ade2-1 can1-100 GAL psi+*	Uhlmann (2000)	Fig 1a, 1b, 1c and 1d
CCG4000	*MATa ura3-52 lys2-801 ade2-101 trp1-Δ63 his3-Δ200 leu2-Δ1 bar1Δ*	Strunnikov lab	
CCG12036	K9027; *TetO:1513Kb ChrIV:ADE2*	This study	Fig 1d
CCG12681	CCG12351; *TetO:1513Kb ChrIV:HIS3*	This study	Fig 1d 2d
CCG12955	CCG12681; SMC3-PK6:HPH	This study	Fig 2a
CCG12356	CCG4000; *MET3-3HA-CDC20:TRP1, FLAG-MCD1-268TEVF-6HA:LEU2, GAL- TEV-9Myc::URA3; tetR-GFP::ADE2*	This study	Fig 2b
CCG12351	CCG4000; *MET3-3HA-CDC20:TRP1*, *FLAG-MCD1-268TEVG-6HA:LEU2*, *GAL1-TEV-9Myc::URA3; tetR-GFP::ADE2*	This study	Fig 2c, 4a, 4b, 4c
CCG12682	CCG12356; *TetO:1513Kb ChrIV:HIS3*	This study	Fig 2d
CCG14783	CCG12351; *TetO:469Kb ChrV:HIS3*	This study	Fig 2d
CCG14784	CCG12356; *TetO:469Kb ChrV:HIS3*	This study	Fig 2d

CCG14820	CCG4000; *MET3-3HA-CDC20:TRP1; ADH1-OsTIR1::URA; MCD1:AID-9Myc:Hph; TetR-GFP::ADE2; TetO:469Kb ChrV:HIS3*	This study	Fig 3a, 3b, 3c
CCG14881	CCG4000; *MET3-3HA-CDC20:TRP1; ADH1-OsTIR1::URA; MCD1:AID-9Myc:Hph; TetR-GFP::ADE2; TetO:558Kb ChrV:HIS3*	This study	Fig 3c
CCG14635	CCG4000; *MET3-3HA-CDC20:TRP1; ADH1-OsTIR1::URA; MCD1:AID-9Myc:hph; TetR-GFP::ADE2; TetO:1513Kb ChrIV:HIS3*	This study	Fig 3d, 4a, 4b, 4c
CCG14629	CCG4000; *MET3-3HA-CDC20:TRP1; ADH1-OsTIR1::URA; MCD1:AID-9Myc:Hph; TetR-GFP::ADE2; TetO:448Kb ChrIV:HIS3*	This study	Fig 3d
CCG14882	CCG14635; SMC3-Pk6:hph	This study	Fig 3e
CCG12925	CCG12682; SMC3-PK6:HPH	This study	Fig 3e
CCG13574	CCG4000, *MET3-3HA-CDC20:TRP1;* p*ADH1-OsTIR1::URA; TetR-GFP::ADE2*	This study	Fig 4a, 4b, 4c
CCG14896	CCG4000; *ADH1-OsTIR1::LEU; CDC15:AID-9Myc:Hph*	This study	Fig 4a, 4b, 4c
CCG14731	*CCG1835; MCD1-6HA:Hyg*	This study	Fig 4d, 4f
CCG14897	CCG4000; *SPC29-RedStar2*:Nat; *SMC3-yeGFP:Hph*; pADH1-OsTIR1::URA	This study	Fig 4e
CCG14898	CCG4000; *SMC3-yeGFP:Hph*; pADH1-OsTIR1::URA	This study	Fig 4e
CCG1835	*MATa bar1:hisG ura3-1 trp1-1 leu2-3,112 his3-11 ade2-1 can1-100 GAL+ cdc15-2*	This study	Fig 4f
CCG14758	CCG4000; *SMC1-6HA:Nat*; pADH1-OsTIR1::URA	Garcia-Luis J. *NSMB* (2019).	Fig 4f
CCG14899	CCG4000 pADH1-OsTIR1::LEU; c*dc15as1:KanMX*	This study	Fig 4g, 4h, 4i
CCG14900	CCG14899 *MCD1:AID-9Myc:Hph*	This study	Fig 4g, 4h, 4i

CCG14901	CCG14900 *SMC3:AID-9Myc:Hph*	This study	Fig 4g, 4h, 4i
CCG14894	*MATa ura3 his3 ade2 cdc20Δ:LEU2 trp:pGAL-CDC20 TRP bar1::natMX4; YCG1-9Myc:Hph; pADH1-OsTIR1::URA*	This study	Fig 5a
CCG14895	CCG14894 *MCD1:AID-9Myc:Kan*	This study	Fig 5a
CCG14892	CCG4000 *YCG1-9Myc:kan; MCD1-9Myc:nat*	This study	Fig 5b, 5c
CCG14486	*MATa his3Δ1 leu2Δ0 lys2Δ0 ura3Δ0; pADH1-OsTIR1:URA; MCD1-6HA:nat; CDC5-AID-9Myc Hyg; YCG1-9Myc:Kan*	This study	Fig 5d
SP493	*MATa his3Δ1 leu2Δ0 met15Δ0 ura3Δ0 trp1::hisG CDC5–6FLAG:kanMX6 aur1::AUR1-C,PGAL1-MCD1-3HA MCD1–9PK:His3MX6*	Pakchuen S. JBC. 2016	Fig 5e
SP494-3	*MATa his3Δ1 leu2Δ0 met15Δ0 ura3Δ0 trp1::hisG CDC5–6FL:kanMX6 aur1::AUR1-C,PGAL1-MCD1-3HA mcd1-S161A, T174A, S183A,S 194A, S195A, T208A, S209A, S211A, T216A, S219A, S220A, T225A, T242A, T250A, S273A-9PK: His3MX6*	Pakchuen S. JBC. 2016	Fig 5e
CCG14898	SP493*; YCG1-9Myc::Hph*	This study	Fig 5f
CCG14899	SP494-3*; YCG1-9Myc::Hph*	This study	Fig 5f
CCG14900	CCG14898 *NET1-yeGFP:TRP; pADH1-OsTIR1::URA; CDC16-AID-9Myc:Nat*	This study	Fig 5g
CCG14901	CCG14899 *NET1-yeGFP:TRP; pADH1-OsTIR1::URA; CDC16-AID-9Myc:Nat*	This study	Fig 5g
CCG14890	CCG4000 *YCG1-9Myc:Kan; GAL-3HA-CDC5::URA*	This study	Fig 6a
CCG14883	CCG4000 *MET3-3HA-CDC20:TRP1*; TetR-GFP:ADE2; TetO ChrIV:1513; Cdc15-AID-9Myc:Nat; pADH1-OsTIR1::LEU; Gal-3HA-Cdc5::URA	This study	Fig 6b, 6c
CCG14884	CCG4000; YCG1-9Myc::Kan; (Cre-EBD78):URA; BRN1:LoxP:1HA_HPH_LoxP:2FLAG:CDC5	This study	Fig 7a, 7b, 8a,

			8b, 8c, 8d, 8e
CCG14885	CCG4000; *YCG1-9Myc::Kan; (Cre-EBD78):URA; BRN1:LoxP:1HA_HPH_LoxP:2FLAG:CDC5KD*	This study	Fig 7a, 7b, 8a, 8b, 8c, 8d, 8e
CCG14902	CCG4000; *YCG1-9Myc::Kan; BRN1:LoxP:2FLAG:CDC5; NET1-yeGFP:TRP; pADH1-OsTIR1::URA; CDC16-AID-9Myc:Hph*	This study	Fig 7c
CCG14903	CCG4000; *YCG1-9Myc::Kan; BRN1:LoxP:2FLAG:CDC5KD; NET1-yeGFP:TRP; pADH1-OsTIR1::URA; CDC16-AID-9Myc:Hph*	This study	Fig 7c
CCG14888	CCG4000 *MET3-3HA-CDC20:TRP1; ADH1-OsTIR1::LEU; CDC15:AID-9Myc:nat; TetR-GFP::ADE2; TetO:1513Kb ChrIV:HIS3;* (Cre-EBD78):URA; BRN1:LoxP:1HA_HPH_LoxP:2FLAG:CDC5	This study	Fig 7d, 7e
CCG14889	CCG4000 *MET3-3HA-CDC20:TRP1; ADH1-OsTIR1::LEU; CDC15:AID-9Myc:nat; TetR-GFP::ADE2; TetO:1513Kb ChrIV:HIS3; (Cre-EBD78):URA; BRN1:LoxP:1HA_HPH_LoxP:2FLAG:CDC5KD*	This study	Fig 7d, 7e
CCG14886	CCG14884; pRS412	This study	Fig 7f
CCG14887	CCG14885; pRS412	This study	Fig 7f

Media, culture conditions and DNA constructs

To arrest the cells in G1, α-factor was added to exponentially growing MATa cultures (OD_{600}=0.5) to a final concentration of 3 x 10-8 M for 3 hours at 25°C. To arrest cells in G2/M, Nocodazole (1.5 mg/mL stock in 100% DMSO) was added to cultures with an OD_{600}=0.5 to a final concentration of 0.015 mg/mL for 2.5 hours. To arrest cells in metaphase (Cdc20), cells carrying the *CDC20* gene under methionine repressible promoter MET3 (*MET3-CDC20*) were grown overnight in minimal media lacking methionine. The day after cells were arrested by washing the cells and resuspending them in rich media containing 5mM methionine for 3 hours. To arrest cells in telophase,

Cdc15 was tagged with an auxin degron (*CDC15-AID*), and IAA was added to the culture at a final concentration of 3mM or 1mM when growing in minimal media. To arrest the cells in late telophase using the cdc15as1 allele, cells released from an alpha factor arrest were treated with 10μM of the ATP analogue 1-NM-PP1 for 1 hour 45 min. To arrest cells in metaphase (*Cdc16*), *CDC16* was tagged with an auxin degron (*CDC16-AID*), and IAA was added to the culture at a final concentration of 3mM for 3 hours at 25ºC. Cultures were monitored by microscopy until ≥90% of cells were arrested. To release cells from G1, the culture was spun (4,000 r.p.m, 1 min) and washed in YPD 3 times. The pellet was then resuspended in YPD containing 0.1 mg/mL pronase. To release cells from Nocodazole, the culture was spun (4,000 r.p.m, 1 min) and washed in YPD containing 1% DMSO 5 times. The pellet was then resuspended in YPD. To degrade proteins tagged with AID epitope, a stock of IAA of 0.6M in ethanol 100% was used. *BRN1-CDC5* DNA construct was design to replace *BRN1* endogenous locus. To induce the fusion between *BRN1* and *CDC5*, β-estradiol was added to the media at 1μM to induce Cre-EBD78 import to the nucleus and act on the loxP secuences located adjacent to *BRN1* and *CDC5*. *CDC5* KEN degradation box, located in N-terminus, was mutated to AAN to avoid interference with the fusion Brn1-Cdc5 degradation [51]. A long linker consisting of KESGSVSSEQLAQFRSLD was introduced between Brn1 and Cdc5 to allow flexibility and solubility. As a control the same construct but with Cdc5 kinase dead (Cdc5-KD) was used.

Microscopy and statistics

To monitor cell cycle progression and chromosome segregation an epifluorescence OLYMPUS IX70 microscope was used fitted with a Lumecor Spectra LED light source, a Hamamatsu Orca Flash 4.0 V2 camera and a 100X/1.35 lens. 1 mL of cell culture was taken from each time point and mixed with glycerol (20% final concentration) to preserve *TetO*/TetR signal after being frozen at -80°C. For visualization, cells were centrifuged at 3,000 r.p.m. for 2 minute and ~1 μL of the pellet was mixed with ~1 μL of DAPI solution (DAPI 4 μg/mL Triton 1 %) on the microscope slide. For each field 20 z-focal planes images were captured (0.3 μm depth between each consecutive image). Images were analysed with Fiji [52]. To quantify the distance between the GFP dots a Fiji macro was developed to automatically compute the

weighted centroid of the dots and measure the three-dimensional distance between them. To visualize Net1-yeGFP or Smc3-yeGFP, cell were imaged fresh in a DELTAVISION Elite fluorescence microscope fitted with a Lumecor Spectra LED light source, a Photometrics Coolsnap HQ camera and a 100x/1.4 lens. Smc3-yeGFP signal intensity was calculated as the ratio of signal at the centromeres and the signal of the same area in the nucleus on Z-projection of images taken every 0.2 µm in 6 µm) Distance between GFP dots were represented in boxplots, where black dots represent the average of each biological repetition, open circles represent each datapoint, centre line represent the median and box limits the 25th and 75th percentile and notches gives roughly 95% confidence interval for comparing medians. At least 80 cells were quantified for each timepoint. Statistical significance of the difference between medians was calculated using Mann-Whitney U test.

Western blot

Protein extraction was done by lysing the cells in a FastPrep FP120 (BIO101) machine with 20% TCA and glass beads. 3 repetitions of a 20 seconds cycle, power setting 5.5. Proteins were precipitated with TCA 7.5% and centrifuging at 15000rpm for 10 min at 4 °C. Then the pellet was resuspended in Laemmli buffer 1.5X. For phosphorylation western blots proteins were resolved in 6.5% Acrylamide 0.17% bisacrylamide, run at 20 mA on ice until the 75 kDa marker reached the bottom of the gel. For the rest of the western blots, 7.5% SDS-PAGE gels were used. Proteins were transferred to polyvinylidene fluoride (PVDF) membranes using the TE70X semidry blotter system (Hoefer). The antibodies used were anti-HA (Roche, 3F10), anti-Myc (Roche, 9E10), anti-PGK1 (Thermo Scientific, 459250) anti-V5 (Abcam, ab9116) and anti-FLAG (Invitrogen MA1-142). Blots were incubated with the ECL Prime Western blotting detection reagent (GE Healthcare). Blots were developed by exposure to high-performance chemiluminescence films (Amersham Hyperfilm ECL, GE Healthcare) or in an ImageQuant LAS 4000 mini machine (GE Healthcare).

FACS

1 millilitre of culture was taken for each time point, pelleted and resuspended in 500 µL of 70% ethanol. Pellets were then resuspended in 250 µL of 1X saline sodium citrate solution (SSC) supplemented with 0.1 mg/mL of RNaseA and incubated overnight at

37 °C. The following day 50 µL of 1X SSC supplemented with 0.6 mg/mL of proteinase K was added to each tube and incubated for 1 hour at 50 °C. Then 250 µL of SSC containing 3 µg/mL propidium iodide was added to each tube and incubated at room temperature for 1 hour. Before FACS analysis cells were sonicated for 5 min in a water bath sonicator (low power, 30 seconds on, 30 seconds off). Finally, 200 µL of each sample was read with a BD LSR II, ensuring 10,000 events per sample.

Sectoring assay

Cells containing a defective *ade2-101* ochre allele of *ADE2* was transformed with a non-essential centromeric plasmid containing a wildtype copy of *ADE2*. Cells that transmit correctly the plasmid to the progeny will form white colonies while the loss of the plasmid will lead to red colonies or red sector. The constructs *BRN1-CDC5* and *BRN1-CDC5KD* were inserted in these cells and grown in adenine-lacking SD medium that retained the plasmid followed by plating on YPD plates or YPD + 1µM β-estradiol to induce the Cre-mediated fusion of *BRN1-CDC5*

Chromatin Immunoprecipitation

For ChIP analysis, cells were grown to an $OD_{600} = 0.5$ and arrested at the required cell cycle stage. A total of 100 OD_{600} units of S. cerevisiae were collected. Cells were fixed for 15 min at 25 °C and quenched with glycine (final concentration 125 mM) for 7 min before cells were harvested by centrifugation at 4,000 r.p.m. for 1 min. The cell pellets were washed in PBS and transferred to a screw cap tube and frozen on dry ice. The pellets were stored at −80 °C. Pellets were resuspended in 300 µl of IP buffer (150 mM NaCl, 50 mM Tris-HCl (pH 7.5), 5 mM EDTA, NP-40 (0.05% vol/vol), Triton X-100 (1% vol/vol)) containing PMSF (final concentration 1 mM) and complete protease inhibitor cocktail (without EDTA, from Roche). A 500 µl volume of glass beads was added to the tubes. Cells were broken in a FastPrep FP120 cell disruptor (BIO101) by three repetitions of a 20 s cycle at power setting 5.5. The cell lysate was transferred to a new tube and 100 µl volume of IP buffer containing PMSF and protease inhibitors was added. The cell lysate was spun down for 10 min at 15,000 r.p.m at 4 °C. This pellet was resuspended in 1 ml of IP buffer containing PMSF and protease inhibitors, and sonicated for 30 (30 s on, 30 s off) at high power at 4 °C in a Diagenode Bioruptor pico. After sonication samples were spun down for 10 min at 15,000 r.p.m. the supernatant

was taken. A 200 µl volume of the sonicated chromatin was taken as 'input' and 400 µl was incubated with 40 µg of anti-V5 antibody (anti-V5 Abcam, ab9116) in a sonicator at low power for 30 min (30 s on, 30 s off). The 'input' DNA was precipitated with 0.3 M sodium acetate and 2.5 volumes of cold ethanol and spun down at 15,000 r.p.m. for 30 min, then the supernatant was removed. The pellet was washed with 70% ethanol and air-dried. After antibody binding, the IP sample was spun down at 13,000 r.p.m for 5 min and the supernatant was added to 60 µl of Dynabeads protein G (Invitrogen), previously equilibrated with IP buffer. The samples were then incubated for 2 h at 4 °C in a rotating wheel and washed five times with IP buffer using a magnetic separator rack. Finally, 'input' samples and IP samples were resuspended in de-crosslinking buffer (TE 1×, 1% SDS, 10 µg ml−1 RNase A, 1 mg ml−1 proteinase K) and incubated at 65 °C overnight. Samples were purified using a ChIP DNA Clean & Concentrator kit (Zymoresearch) according to the manufacturer's instructions. Calibrated ChIP-seq were done as described in [10].

Protein co-immunoprecipitation

120 OD_{600} of asynchronous cells were $OD_{600} = 1$ were collected and washed in cold water and resuspended in 200 µl of ice-cold buffer A (50 mM HEPES, 150 mM KCl, 1.5 mM $MgCl_2$, 0.5 mM DTT and 0.5% Triton X-100 (pH 7.5) supplemented with complete protease inhibitor cocktail tablets (Roche)). 500 ml of glass beads (425-600 µm) were added and cells lysed in a FastPrep FP120 cell disruptor (BIO101) by 3 repetitions of a 20 s cycle at power setting 5.5. Extracts were maintained on ice for 2 min after each cycle. Cell extracts were centrifuged for 10 min at 12000 r.p.m at 4C and the supernatant incubated with protein G Dynabeads (Invitrogen) bound to anti-Myc antibody (Roche, 9E10) for 2 h at 4 °C. Finally, beads were washed five times in washing buffer (10 mM Tris-Cl pH 7.5, 150 mM NaCl, 0.5% Triton X-100) and unbound from the antibody by incubating at 37°C for 4 min in SR buffer (2% SDS, 0.125 M Tris-Cl pH 6.8). Immunoprecipitated proteins were mixed with SS buffer (5% saccharose, 0.0125% bromophenol blue) and run in an SDS–PAGE gel.

Hi-C libraries

Cells were fixed with 3% formaldehyde (Sigma-Aldrich, F8775) as detailed in [53]. Formaldehyde was quenched with 300 mM of glycine at room temperature for 20 min.

Hi-C experiments were performed with a Hi-C kit (Arima Genomics) involving a double DpnII + HinfI restriction digestion. Preparation of the samples for paired-end sequencing on an Illumina NextSeq500 (2x35 bp) was done with Collibri™ ES DNA Library Prep Kit for Illumina Systems (Thermo Fisher, A38605024).

Generation and normalization of contact maps

Alignment of the reads and processing of the contact data was done with Hicstuff using the S288C reference genome [54]. Hicstuff pipeline was launched with the following parameters: filter out spurious 3C events, filter out PCR duplicates based on read positions. The "view" mode of Hicstuff SCN function was used to generate normalized contact maps as described in [55]. Contact maps were binned at 50kb for the whole genome or 1kb for single chromosomes, and 30 kb for single chromosome ratio map.

Contact probability as a function of the genomic distance P(s)

Genome-wide contact probability as a function of genomic distance Pc(s) and its derivative were computed using the "distance law" function of Hicstuff with default parameters, averaging the contact data of entire chromosome arms [54]. For pre-rDNA region, contact probability as a function of genomic distance Pc(s) and its derivative were computed after alignment of the reads against the 290kb long pre- and post-rDNA region, as if they were individual chromosomes.

Aggregated of *cis* and *trans* centromere contacts

Cis-centromere pile-up contact maps are the result of averaged 205 kb windows with a bin of 5 kb generated with Chromosight in quantify mode (option: --pattern border, --perc-zero=100) [54] centered on the 16 centromere position, and divided by the mean for each pixel of its diagonal. *Trans*-centromere pile-up were similarly generated by Chomosight, but with the option --inter, and centered on centromere intersections.

Figure legends

Figure 1. Mcd1 cleavage by TEV protease leads to bulk chromosome segregation

a, Schematic of engineered *MCD1* with the wild-type separase cleavage site maintained in the position 180 and the cleavage position 268 replaced by the TEV cleavage sequence ENLYFQG (upper panel). Cells with this engineered *MCD1* were synchronised in Cdc20 metaphase arrest and induced to express TEV protease. Samples were taken every 30 min for 3 hours for Western blotting against HA epitope in the C-terminus of Mcd1 (lower panel). **b**, Bulk chromosome segregation was monitored by looking at DNA DAPI staining of cells treated as in a. **c**, Representative photos of cells with segregated centromere proximal GFP tag on chromosome V containing DNA bridges observed by DAPI staining. **d,** Cells treated as in a, with a centromere proximal GFP tag on chromosome V or a subtelomeric GFP tag on chromosome IV were monitored for tag segregation taking samples every 30 min for 2 hours (left panel). Representative images of cells with a centromere proximal GFP tag on chromosome V and a subtelomeric GFP tag on chromosome IV with mis-segregated tags (right panel).

Figure 2. Stability of Mcd1 cleavage fragment affects fidelity of chromosome segregation

a, Schematic of engineered cohesin with *MCD1* tagged in N-terminus with FLAG, the C-terminus with HA, substituting the 268 separase cleaving position by the TEV cleavage sequence ENLYFQG (TEVG) and with Smc3 tagged at the C-terminus with V5 (left panel). Cells with this engineered cohesin were synchronised in Cdc20 metaphase arrest and Mcd1 was cleaved at the TEV cleavage site. Samples were taken every 30 min for 2 hours and Smc3-PK6 was pulled down using anti-V5 antibody followed by FLAG or HA immunoblotting to detect Mcd1 N-terminus and C-terminus cleaved fragments respectively (right panel). **b**, Cells with *MCD1* tagged at its N-terminus with FLAG and its C-terminus with HA, and with the 268 separase cleaving position replaced with the TEV cleavage sequence ENLYFQF (TEVF) were arrested in Cdc20 and Mcd1 was cleaved in the TEV cleaving site. Samples were taken every 30 min for 2 hours and immunoblotted against FLAG or HA to detect Mcd1 N-terminus and C-terminus cleaved fragments respectively (left panel). Chromosome segregation was monitored by looking at DNA DAPI staining (right panel) **c**, Cells with *MCD1*

tagged at its N-terminus with FLAG and its C-terminus with HA, and with the 268 separase cleaving position replaced with the TEV cleavage sequence ENLYFQG (TEVG) were treated as in b and samples were taken every 30 minutes for two hours. Samples were immunoblotted against FLAG or HA to detect *MCD1* N-terminus and C-terminus cleaved fragments respectively (left panel). Chromosome segregation was monitored by looking at DNA DAPI staining (right panel) **d**, Cells carrying *MCD1* with the 268 separase cleaving position substituted by the TEV cleavage sequence ENLYFQF (TEVF) or ENLYFQG (TEVG) were treated as in b and monitored for segregation of GFP dots marking the middle of chromosome V (top left) or the subtelomere of the right arm of chromosome IV (top middle). Quantifications of cell cycle stage are shown underneath (bottom left and bottom middle). Representative examples of tag segregation are shown (right).

Figure 3. Mcd1 degradation causes catastrophic chromosome segregation

a, Cells containing *MCD1* tagged with the auxin degron (*MCD1-AID*) were arrested in metaphase Cdc20 arrest. The culture was split in two, one of them was treated with DMSO 1% and the other with 6mM of the auxin IAA to degrade Mcd1-AID. Samples were taken for WB analysis every hour, for 3 hours followed by anti-Myc immunoblotting to detect Mcd1. **b,** Representative photos of cells synchronised in Cdc20 arrest and at different times after adding IAA to degrade Mcd1-AID, containing a GFP dot marking the middle of the right arm of chromosome V. **c,** Cells treated as in a, were monitored for segregation of DAPI stained DNA and GFP dots marking the middle of chromosome V (upper panel) or the subtelomere of the right arm of chromosome V (lower panel) **d,** Cells treated as in a, but taking samples every 30 min for 2 hours, were monitored for segregation of DAPI stained DNA and GFP dots marking the centromeric region of chromosome IV (left upper panel) or the subtelomere of the right arm of chromosome IV (left lower panel). Samples for WB analysis where taken in parallel followed by anti-Myc immunoblotting to detect Mcd1 (right panel) **e,** Chromatin-immunoprecipitation analysis (ChIP) of Smc3-Pk6 binding along chromosome V of cells synchronised in Cdc20 metaphase arrest containing either *MCD1* with the 268 separase cleaving position substituted by the TEV cleavage sequence ENLYFQF (TEVF) or with the *MCD1-AID* auxin degron. Samples were taken every 30 min for 1 hour after induction of the TEV protease or addition of the auxin IAA respectively.

Figure 4. Cohesin has a structural role after metaphase

a, Cells containing either *MCD1-TEVG or MCD1-AID* were arrested in Cdc20 metaphase arrest and MCD1 was cleaved or degraded respectively. Samples for WB analysis were taken every 30 min for 2 hours followed by immunoblotting to detect Mcd1. Samples at the timepoints highlighted in red (*MCD1 TEVG* 90 min. cleavage and *MCD1-AID* 60 min degradation) were taken to be processed for HiC (top). The cell cycle stage of these samples was quantified. Cell synchronised in Cdc20 were included as a control (bottom left). Representative cell images of each sample are shown (bottom right). **b**, Contact maps (bin = 1kb) of chromosome V from cell populations treated as in a. Cdc20 metaphase arrest, Cdc20 arrested cells with *MCD1 TEV-G* cleaved for 90 min, Cdc20 arrested cells with *MCD1-AID* degraded for 60 min. Brown to yellow colour scales represent high to low contact frequencies, respectively (log10) **c**, Average intra-chromosomal contact frequency (P) between two loci with respect to their genomic distance (s) along the chromosome, of cell populations treated as in "a" (left). Derivative of P(s) curve (right). **d**, Cells containing the temperature sensitive allele *cdc15-2* and tagged Mcd1-9Myc were arrested in G1 and released into media containing nocodazole to arrest the cells in metaphase. Subsequently nocodazole was washed out and cells were arrested in *cdc15-2* late anaphase by increasing the temperature to 37C. Finally, cells were released from *cdc15-2* arrest to cycle by decreasing the temperature back to 25C. Samples for Western blot analysis were taken at the indicated timepoints followed by anti-Myc immunoblotting to detect Mcd1. Short (top) and long (middle) exposure are shown to show Mcd1 full length (short exposure) and Mcd1 cleavage fragments (long exposure). Immunoblotting to detect Pgk1 was used as a loading control (bottom). FACS analysis of the same experiment (middle). Representative images of the experiment are shown (right). **e**, Cells containing *CDC15-AID* and the tagged cohesin subunit *SMC3-yeGFP* were arrested in Cdc15 late anaphase and the GFP signal at the centromere was calculated as a ratio compared to the nuclear background signal. Cells also containing the tagged spindle pole body component Spc29-RedStar2 were used as spatial reference to determine colocalization with centromeres. **f**, Cells containing *cdc15-as* and *NET1*-yeGFP and with either MCD1 WT or the temperature sensitive allele *mcd1-73*, were arrested in telophase (*cdc15-as*) at 25°C and then temperature was shifted to 37°C for 30 min and imaged under the

microscope. Representative images of the experiment are shown (top). Net1-GFP area marking the rDNA was quantified (bottom left). Quantification of the rDNA morphology (bottom right). **g**, Enrichment of cohesin along a 650 kb region of *S. cerevisiae* chromosome 7 measured by calibrated ChIP-seq in cells containing SMC1-6HA arrested in metaphase (nocodazole), untagged cells arrested in metaphase (nocodazole), cells containing *MCD1-6HA* arrested in *cdc15-2* late anaphase and untagged cells arrested in *cdc15-2* (top 4 blue lanes). The two bottom black lanes show the enrichment of cohesin subunit Smc1-6HA and Mcd1-6HA after subtraction of ChIP-seq signal of the untagged cells arrested in metaphase or *cdc15-2* respectively. *CEN7* marks the location of the centromere. The average signal of the number of reads at each base pair from the centromere CDEIII region of the 16 chromosomes is shown (bottom), **h**, Log_2-ratio of contact maps between G1 (alpha factor) arrested cells and late telophase arrested cells (*cdc15as*) (left), Log_2-ratio of contact maps between *cdc15as* arrested cells and *cdc15as* arrested cells depleted in Mcd1 (right, top-half of the matrix) or Mcd1 and Smc3 (right, bottom-half of the matrix). x and y axis represent the 16 chromosomes of the yeast genome depicted on top of the matrix. Blue to red colour scales represent the enrichments in contacts in one sample respect to the other (bin=50kb).**i-j**, Pile-ups of contact maps of the 100 kb peri-centromeric regions in cis (h) or in trans (i) for cells synchronised in *cdc15as* (left), cells synchronised in *cdc15as* and Mcd1 depleted (middle) cells synchronised in *cdc15as* and Mcd1 and Smc3 depleted (right). Log2-ratio of contact maps between *cdc15as* and *cdc15as* Mcd1 depleted (far right, top-half of the matrix) and *cdc15as* and *cdc15as* Mcd1 Smc3 depleted (far right, bottom-half of the matrix)

Figure 5. Cohesin levels regulate condensin phosphorylation

a, Cells containing WT *MCD1 or MCD1* tagged with the auxin degron (*MCD1-AID*) were arrested in G1 with α-factor and released to Cdc20. At indicated timepoints samples were taken for phosphorylation Western blot analysis followed by anti-Myc immunoblot to detect Ycg1 (left). Quantification of the ratio Ycg1·P/Ycg1 of two independent experiments (right). Data represent the average of two replicates and error bars represent S.D **b,** Cells synchronised in metaphase using nocodazole, were release into fresh medium and samples were taken for phosphorylation WB analysis and immunoblot to detect Ycg1 and Mcd1 (left panel). Quantification of the ratio

Ycg1·P/Ycg1 and Mcd1 levels (right). **c,** Cells containing *MCD1-AID* were synchronised in metaphase using nocodazole and IAA was added to degrade Mcd1-AID. At indicated time points samples were taken and processed for phosphorylation WB analysis followed by anti-Myc immunoblot to detect Ycg1 **d,** Cells containing *CDC5-AID* were synchronised in in metaphase using nocodazole, the culture was split in two and one treated with DMSO and the other with IAA to degrade Cdc5-AID. Samples were taken at the indicated time points for phosphorylation WB analysis and immunoblotted to detect Ycg1 and Cdc5 **e,** Immunoprecipitation of Mcd1-pk6 or Mcd1-15A-Pk6 via Pk6 epitope. Mcd1-Pk6 and Cdc5-FLAG were detected in the immunoprecipitated (IP), however when immunoprecipitating Mcd1-15A-Pk6, Cdc5-FLAG is barely detected in the IP **f**, Cells containing WT *MCD1 or mcd1-15A* were arrested in G1 with α-factor and released to metaphase using nocodazole. At indicated timepoints samples were taken for phosphorylation WB analysis followed by anti-Myc immunoblot to detect Ycg1 (top). Quantification of the ratio Ycg1·P/Ycg1 (bottom left). FACS analysis of the same experiment taking samples every 15 min (bottom right)

Figure 6. Cdc5 overexpression promotes condensin hyperphosphorylation and lagging chromosomes during segregation.

a, Cells with integrated *GAL-3HA-CDC5* were arrested in metaphase using nocodazole and Cdc5 expression was induced by adding galactose to the culture for 1 hour. Samples were taken before and after the induction for phosphorylation WB analysis followed by anti-Myc and anti-HA immunoblot to detect Ycg1-Myc and HA-Cdc5 respectively. **b,** Cells with GFP dots marking the subtelomere of the right arm of chromosome IV and with integrated *GAL-3HA-CDC5* were synchronised in Cdc20 metaphase and split in two, glucose was added to one culture and galactose to the other to repress or induce the expression of Cdc5 respectively and released into a Cdc15 arrest. Samples were taken at the indicated timepoints to assess DAPI stained DNA segregation and GFP dots segregation. **c,** In cells treated as in b, the three-dimensional distance of the weighted centroid of the GFP dots was measured at the indicated timepoints. Black dots represent the average of each biological repetition. 45 min ****: $p=2.2*10^{-16}$ 60min **** $p =6.6*10^{-16}$ Mann Whitney Test.

Figure 7. Constitutively hyperphosphorylated condensin causes lagging chromosomes during segregation and genomic instability

a, Schematic of the engineered gene loci coding for Brn1-Cdc5 or Brn1-Cdc5KD (kinase dead) before and after the Cre recombinase mediated fusion (left). Growth test analysis of Brn1-Cdc5 or Brn-Cdc5KD growing in YPD (proteins not fused) or YPD + β-estradiol (proteins fused). Plates were incubated at 30°C for 48h (right) **b,** Cells containing Brn1-Cdc5 or Brn1-Cdc5KD were synchronised in G1 with α-factor and released, taking samples at the indicated timepoints for phosphorylation WB analysis followed by anti-Myc immunoblot to detect Ycg1-Myc and anti-FLAG immunoblot to detect Brn1-FLAG-Cdc5 or Brn-FLAG-Cdc5KD (left). Quantification of the ratio Ycg1·P/Ycg1 and Brn-Cdc5·P/Brn1-Cdc5 in cells expressing Brn1-Cdc5 or Brn1-Cdc5KD (middle). FACS analysis of the same experiment (right) **c,** Cells with either the fusion Brn1-Cdc5 or Brn-Cdc5KD were synchronised in G1 and released into a Cdc15 arrest. Samples were taken at the indicated timepoints and cell cycle progression was monitored with DAPI stained DNA and GFP dots segregation marking the subtelomere of the right arm of chromosome IV. **d**, Cells with GFP dots marking the subtelomere of the right arm of chromosome IV and either the fusion Brn1-Cdc5 or Brn-Cdc5KD were synchronised in G1 and released into a Cdc15 arrest. Samples were taken at the indicated timepoints to measure the three-dimensional distance of the weighted centroid of the GFP dots. Black dots represent the average of each biological repetition. n.s. Non significative, 105 min ****: $p=6.9*10^{-7}$, 120 min **** $p =1.1*10^{-11}$, 135 min *** $p =2.1*10^{-4}$. Mann Whitney Test. **e**, Sectoring assay for the chromosome loss using a strain containing Brn1-Cdc5 or Brn1-Cdc5KD **f,** Cells containing *NET1*-yeGFP, *CDC16-AID* and *BRN1-CDC5* or *BRN1-CDC5KD* were arrested in metaphase (Cdc16) by adding auxin to the media. Representative images are shown. White scale bar represents 5 μm. BF, bright field (left). rDNA length was quantified. Box plot of the quantification of the length of the rDNA. Black dots represent the average of each biological repetition, open circles represent each datapoint, centre line represent the median and box limits the 25th and 75th percentile. Notches gives roughly 95% confidence interval for comparing medians. ****: $p=2.2*10^{-16}$ Mann Whitney Test (right).

Figure 8. Cells with constitutively hyperphosphorylated condensin exhibit structural defects

a, Contact maps generated from cell containing Brn1-Cdc5 or Brn1-Cdc5KD arrested in metaphase (nocodazole). x- and y-axis represent the 16 chromosomes of the yeast genome, displayed above the maps. Brown to yellow colour scales represent high to low contact frequencies, respectively (log10) (left). Log_2-ratio of contact maps between Brn1-Cdc5 and Brn1-Cdc5KD (right) **b-c**, Pile-ups of contact maps of the 100 kb peri-centromeric regions *in cis* (b) or *in trans* (c) for cells synchronised in metaphase (nocodazole) and containing Brn1-Cdc5 fusion (left) or Brn1-Cdc5KD fusion (middle). Log_2-ratio of contact maps between Brn1-Cdc5 and Brn1-Cdc5KD (right) **d,** Log_2-ratio of chromosome XII contact maps between Brn1-Cdc5 and Brn1-Cdc5KD **e**, Average intra-chromosomal contact frequency (P(s)) of the 290 kb of the pre-rDNA region (highlighted in yellow) of chromosome XII for cells containing Brn1-Cdc5 fusion or Brn1-Cdc5KD and arrested in metaphase (nocodazole) **f**, Model showing how cohesin fine-tuned cleavage by separase, release Cdc5 producing hyperphosphorylation of condensin. Condensin acquires a more prevalent role in chromosome organization while a small amount of residual cohesin is left interacting with the DNA maintaining a structural role.

References

1. Guacci, V., Hogan, E. & Koshland, D. Chromosome condensation and sister chromatid pairing in budding yeast. *J Cell Biol* **125**, 517-530 (1994).
2. Guacci, V., Koshland, D. & Strunnikov, A. A direct link between sister chromatid cohesion and chromosome condensation revealed through the analysis of MCD1 in S. cerevisiae. *Cell* **91**, 47-57 (1997).
3. Michaelis, C., Ciosk, R. & Nasmyth, K. Cohesins: chromosomal proteins that prevent premature separation of sister chromatids. *Cell* **91**, 35-45 (1997).
4. Nasmyth, K. Disseminating the genome: joining, resolving, and separating sister chromatids during mitosis and meiosis. *Annu Rev Genet* **35**, 673-745 (2001).
5. Uhlmann, F., Lottspeich, F. & Nasmyth, K. Sister-chromatid separation at anaphase onset is promoted by cleavage of the cohesin subunit Scc1. *Nature* **400**, 37-42 (1999).
6. Uhlmann, F., Wernic, D., Poupart, M.A., Koonin, E.V. & Nasmyth, K. Cleavage of cohesin by the CD clan protease separin triggers anaphase in yeast. *Cell* **103**, 375-386 (2000).

7. Rao, H., Uhlmann, F., Nasmyth, K. & Varshavsky, A. Degradation of a cohesin subunit by the N-end rule pathway is essential for chromosome stability. *Nature* **410**, 955-959 (2001).
8. Lazar-Stefanita, L. *et al.* Cohesins and condensins orchestrate the 4D dynamics of yeast chromosomes during the cell cycle. *EMBO J* **36**, 2684-2697 (2017).
9. Schalbetter, S.A. *et al.* SMC complexes differentially compact mitotic chromosomes according to genomic context. *Nat Cell Biol* **19**, 1071-1080 (2017).
10. Garcia-Luis, J. *et al.* FACT mediates cohesin function on chromatin. *Nat Struct Mol Biol* **26**, 970-979 (2019).
11. Rao, S.S.P. *et al.* Cohesin Loss Eliminates All Loop Domains. *Cell* **171**, 305-320 e324 (2017).
12. Sumara, I., Vorlaufer, E., Gieffers, C., Peters, B.H. & Peters, J.M. Characterization of vertebrate cohesin complexes and their regulation in prophase. *J Cell Biol* **151**, 749-762 (2000).
13. Gibcus, J.H. *et al.* A pathway for mitotic chromosome formation. *Science* **359** (2018).
14. Freeman, L., Aragon-Alcaide, L. & Strunnikov, A. The condensin complex governs chromosome condensation and mitotic transmission of rDNA. *J Cell Biol* **149**, 811-824 (2000).
15. Davidson, I.F. *et al.* DNA loop extrusion by human cohesin. *Science* **366**, 1338-1345 (2019).
16. Kim, Y., Shi, Z., Zhang, H., Finkelstein, I.J. & Yu, H. Human cohesin compacts DNA by loop extrusion. *Science* **366**, 1345-1349 (2019).
17. Ganji, M. *et al.* Real-time imaging of DNA loop extrusion by condensin. *Science* **360**, 102-105 (2018).
18. Kong, M. *et al.* Human Condensin I and II Drive Extensive ATP-Dependent Compaction of Nucleosome-Bound DNA. *Mol Cell* **79**, 99-114 e119 (2020).
19. Ono, T. *et al.* Differential contributions of condensin I and condensin II to mitotic chromosome architecture in vertebrate cells. *Cell* **115**, 109-121 (2003).
20. Kimura, K., Hirano, M., Kobayashi, R. & Hirano, T. Phosphorylation and activation of 13S condensin by Cdc2 in vitro. *Science* **282**, 487-490 (1998).
21. Lavoie, B.D., Hogan, E. & Koshland, D. In vivo dissection of the chromosome condensation machinery: reversibility of condensation distinguishes contributions of condensin and cohesin. *J Cell Biol* **156**, 805-815 (2002).
22. St-Pierre, J. *et al.* Polo kinase regulates mitotic chromosome condensation by hyperactivation of condensin DNA supercoiling activity. *Mol Cell* **34**, 416-426 (2009).
23. Robellet, X. *et al.* A high-sensitivity phospho-switch triggered by Cdk1 governs chromosome morphogenesis during cell division. *Genes Dev* **29**, 426-439 (2015).
24. Leonard, J. *et al.* Condensin Relocalization from Centromeres to Chromosome Arms Promotes Top2 Recruitment during Anaphase. *Cell Rep* **13**, 2336-2344 (2015).
25. Renshaw, M.J. *et al.* Condensins promote chromosome recoiling during early anaphase to complete sister chromatid separation. *Dev Cell* **19**, 232-244 (2010).
26. Lamothe, R., Costantino, L. & Koshland, D.E. The spatial regulation of condensin activity in chromosome condensation. *Genes Dev* **34**, 819-831 (2020).

27. Sullivan, M. & Uhlmann, F. A non-proteolytic function of separase links the onset of anaphase to mitotic exit. *Nat Cell Biol* **5**, 249-254 (2003).
28. Higuchi, T. & Uhlmann, F. Stabilization of microtubule dynamics at anaphase onset promotes chromosome segregation. *Nature* **433**, 171-176 (2005).
29. Clemente-Blanco, A. *et al.* Cdc14 phosphatase promotes segregation of telomeres through repression of RNA polymerase II transcription. *Nat Cell Biol* **13**, 1450-1456 (2011).
30. Varshavsky, A. The N-end rule pathway and regulation by proteolysis. *Protein Sci* **20**, 1298-1345 (2011).
31. Beckouet, F. *et al.* Releasing Activity Disengages Cohesin's Smc3/Scc1 Interface in a Process Blocked by Acetylation. *Mol Cell* **61**, 563-574 (2016).
32. Nishimura, K., Fukagawa, T., Takisawa, H., Kakimoto, T. & Kanemaki, M. An auxin-based degron system for the rapid depletion of proteins in nonplant cells. *Nat Methods* **6**, 917-922 (2009).
33. Jaspersen, S.L., Charles, J.F., Tinker-Kulberg, R.L. & Morgan, D.O. A late mitotic regulatory network controlling cyclin destruction in Saccharomyces cerevisiae. *Mol Biol Cell* **9**, 2803-2817 (1998).
34. Alexandru, G., Uhlmann, F., Mechtler, K., Poupart, M.A. & Nasmyth, K. Phosphorylation of the cohesin subunit Scc1 by Polo/Cdc5 kinase regulates sister chromatid separation in yeast. *Cell* **105**, 459-472 (2001).
35. Pakchuen, S., Ishibashi, M., Takakusagi, E., Shirahige, K. & Sutani, T. Physical Association of Saccharomyces cerevisiae Polo-like Kinase Cdc5 with Chromosomal Cohesin Facilitates DNA Damage Response. *J Biol Chem* **291**, 17228-17246 (2016).
36. Botchkarev, V.V., Jr. & Haber, J.E. Functions and regulation of the Polo-like kinase Cdc5 in the absence and presence of DNA damage. *Curr Genet* **64**, 87-96 (2018).
37. Schmitt, A.D., Hu, M. & Ren, B. Genome-wide mapping and analysis of chromosome architecture. *Nat Rev Mol Cell Biol* **17**, 743-755 (2016).
38. Dekker, J., Marti-Renom, M.A. & Mirny, L.A. Exploring the three-dimensional organization of genomes: interpreting chromatin interaction data. *Nat Rev Genet* **14**, 390-403 (2013).
39. Ciosk, R. *et al.* Cohesin's binding to chromosomes depends on a separate complex consisting of Scc2 and Scc4 proteins. *Mol Cell* **5**, 243-254 (2000).
40. Uhlmann, F. & Nasmyth, K. Cohesion between sister chromatids must be established during DNA replication. *Curr Biol* **8**, 1095-1101 (1998).
41. Rolef Ben-Shahar, T. *et al.* Eco1-dependent cohesin acetylation during establishment of sister chromatid cohesion. *Science* **321**, 563-566 (2008).
42. Unal, E. *et al.* A molecular determinant for the establishment of sister chromatid cohesion. *Science* **321**, 566-569 (2008).
43. Cohen-Fix, O., Peters, J.M., Kirschner, M.W. & Koshland, D. Anaphase initiation in Saccharomyces cerevisiae is controlled by the APC-dependent degradation of the anaphase inhibitor Pds1p. *Genes Dev* **10**, 3081-3093 (1996).
44. Waizenegger, I.C., Hauf, S., Meinke, A. & Peters, J.M. Two distinct pathways remove mammalian cohesin from chromosome arms in prophase and from centromeres in anaphase. *Cell* **103**, 399-410 (2000).
45. Tanaka, T., Fuchs, J., Loidl, J. & Nasmyth, K. Cohesin ensures bipolar attachment of microtubules to sister centromeres and resists their precocious separation. *Nat Cell Biol* **2**, 492-499 (2000).

46. Srinivasan, M. *et al.* The Cohesin Ring Uses Its Hinge to Organize DNA Using Non-topological as well as Topological Mechanisms. *Cell* **173**, 1508-1519 e1518 (2018).
47. Baxter, J. *et al.* Positive supercoiling of mitotic DNA drives decatenation by topoisomerase II in eukaryotes. *Science* **331**, 1328-1332 (2011).
48. Sen, N. *et al.* Physical Proximity of Sister Chromatids Promotes Top2-Dependent Intertwining. *Mol Cell* **64**, 134-147 (2016).
49. Thadani, R., Kamenz, J., Heeger, S., Munoz, S. & Uhlmann, F. Cell-Cycle Regulation of Dynamic Chromosome Association of the Condensin Complex. *Cell Rep* **23**, 2308-2317 (2018).
50. Janke, C. *et al.* A versatile toolbox for PCR-based tagging of yeast genes: new fluorescent proteins, more markers and promoter substitution cassettes. *Yeast* **21**, 947-962 (2004).
51. Arnold, L., Hockner, S. & Seufert, W. Insights into the cellular mechanism of the yeast ubiquitin ligase APC/C-Cdh1 from the analysis of in vivo degrons. *Mol Biol Cell* **26**, 843-858 (2015).
52. Schindelin, J. *et al.* Fiji: an open-source platform for biological-image analysis. *Nat Methods* **9**, 676-682 (2012).
53. Dauban, L. *et al.* Regulation of Cohesin-Mediated Chromosome Folding by Eco1 and Other Partners. *Mol Cell* **77**, 1279-1293 e1274 (2020).
54. Matthey-Doret, C. *et al.* Computer vision for pattern detection in chromosome contact maps. *Nat Commun* **11**, 5795 (2020).
55. Cournac, A., Marie-Nelly, H., Marbouty, M., Koszul, R. & Mozziconacci, J. Normalization of a chromosomal contact map. *BMC Genomics* **13**, 436 (2012).

Acknowledgements. We thank members of our laboratories for discussion and critical reading of the manuscript. We thank Helle D Ulrich for kindly sharing the plasmids for auxin-inducible degron tagging. We thank Takashi Sutani for kindly sharing the strains containing the allele mcd1-15A and its WT counterpart. We also thank MRC-LMS microscopy facility for help with the microscope set-up and especially Chad Whilding for developing the Fiji macro for automated distance quantification of GFP dots.

Funding. The work in the Aragon laboratory was supported by the Medical Research Council (UKRI MC-A652-5PY00) and the Wellcome Trust (100955/Z/13/Z). This research was further supported by funding from The European Research Council (R.K.), Agence Nationale pour la Recherche (R.K.).

Author contributions: J.G.L. performed all experiments except for HiC analyses. H.B. and A.T performed HiC experiments and analysis. H.B analysed HiC data. L.A. and J.G-L. conceived the project. L.A. wrote the manuscript. L.A. and R.K. supervised the projects and revised the manuscript.

Competing interests: The authors declare that they have no competing interests.

Data and materials availability: All data needed to evaluate the conclusions in the paper are present in the paper and/or the Supplementary Materials. Additional data related to this paper may be requested from the authors.

Figure 1

a

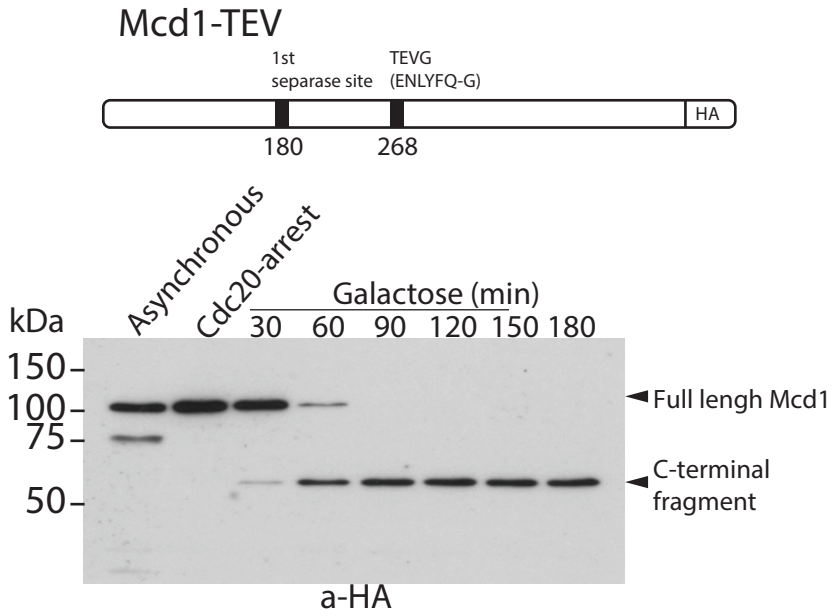

b

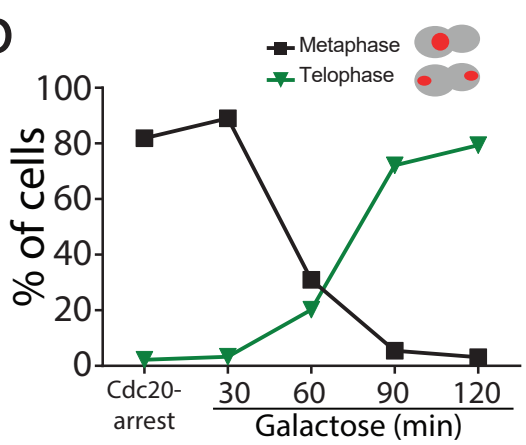

c

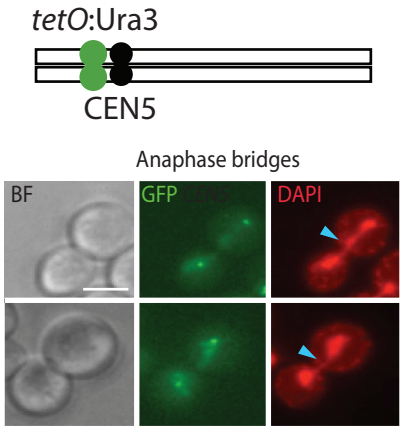

d

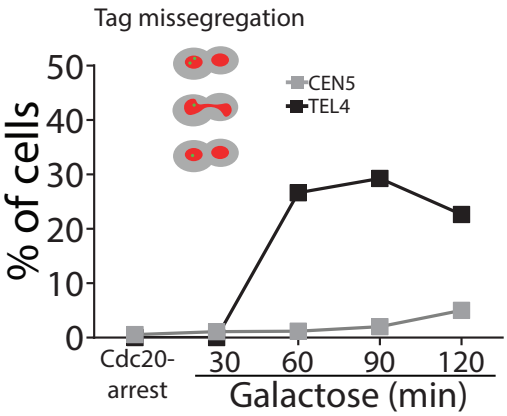

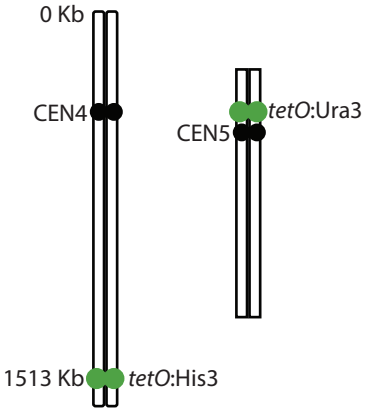

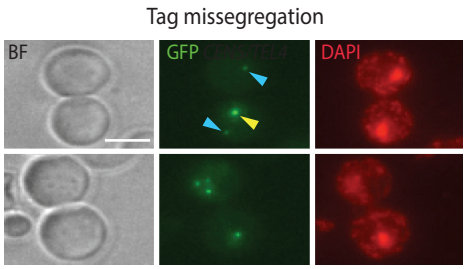

Figure 2

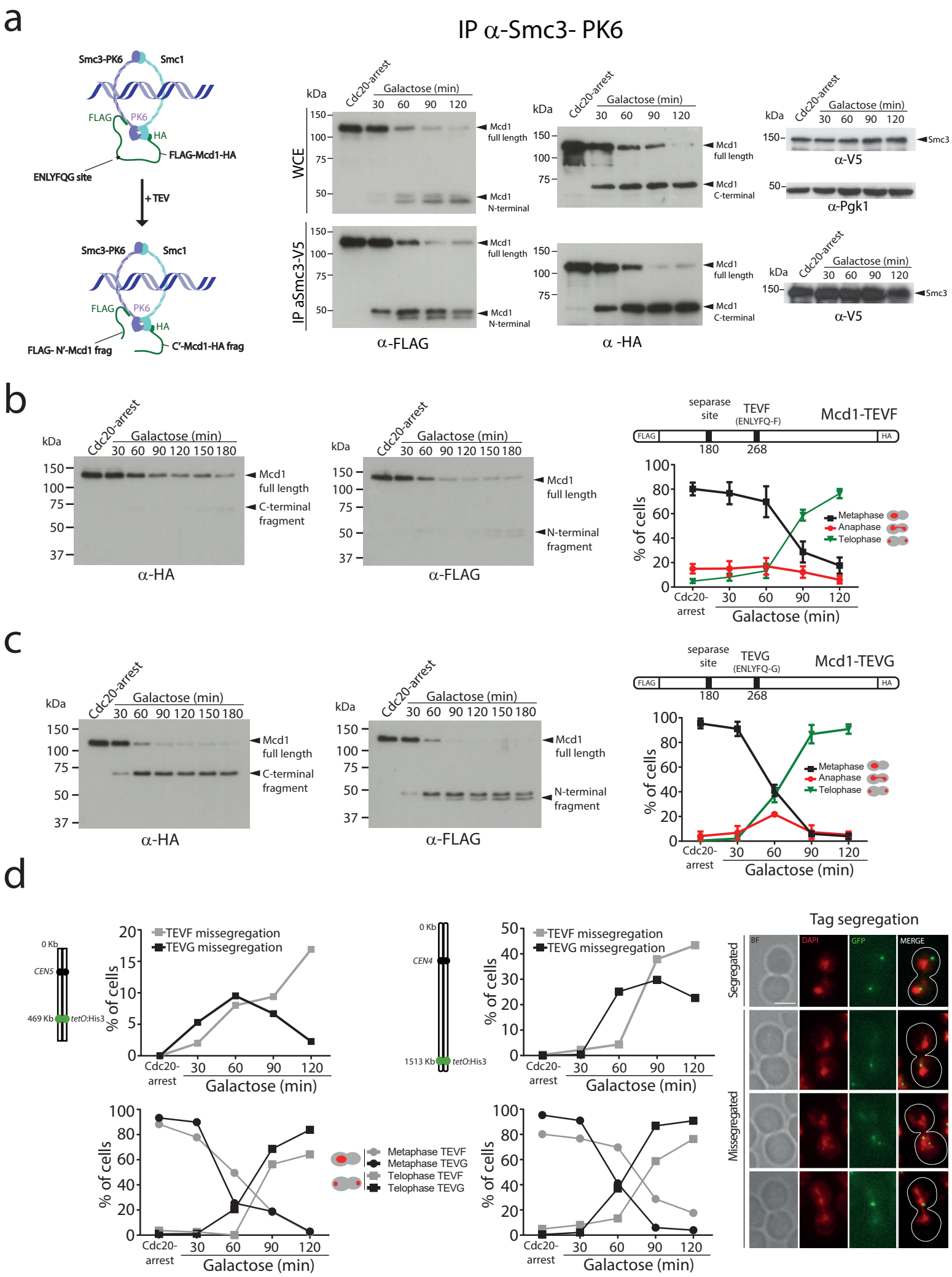
a
IP α-Smc3- PK6
Smc3-PK6
Smc1
FLAG
PK6
HA
FLAG-Mcd1-HA
ENLYFQG site
+TEV
FLAG- N'-Mcd1 frag
C'-Mcd1-HA frag
kDa
Cdc20-arrest
Galactose (min)
30 60 90 120
WCE
IP aSmc3-V5
Mcd1 full length
Mcd1 N-terminal
Mcd1 C-terminal
Smc3
α-V5
α-Pgk1
α-FLAG
α -HA
b
Cdc20-arrest
Galactose (min)
30 60 90 120 150 180
Mcd1 full length
C-terminal fragment
N-terminal fragment
α-HA
α-FLAG
separase site
TEVF (ENLYFQ-F)
Mcd1-TEVF
FLAG
HA
180
268
% of cells
Metaphase
Anaphase
Telophase
Cdc20-arrest
Galactose (min)
c
TEVG (ENLYFQ-G)
Mcd1-TEVG
d
0 Kb
CEN5
469 Kb
tetO:His3
TEVF missegregation
TEVG missegregation
% of cells
Cdc20-arrest
Galactose (min)
CEN4
1513 Kb
Metaphase TEVF
Metaphase TEVG
Telophase TEVF
Telophase TEVG
Tag segregation
BF
DAPI
GFP
MERGE
Segregated
Missegregated

Figure 3

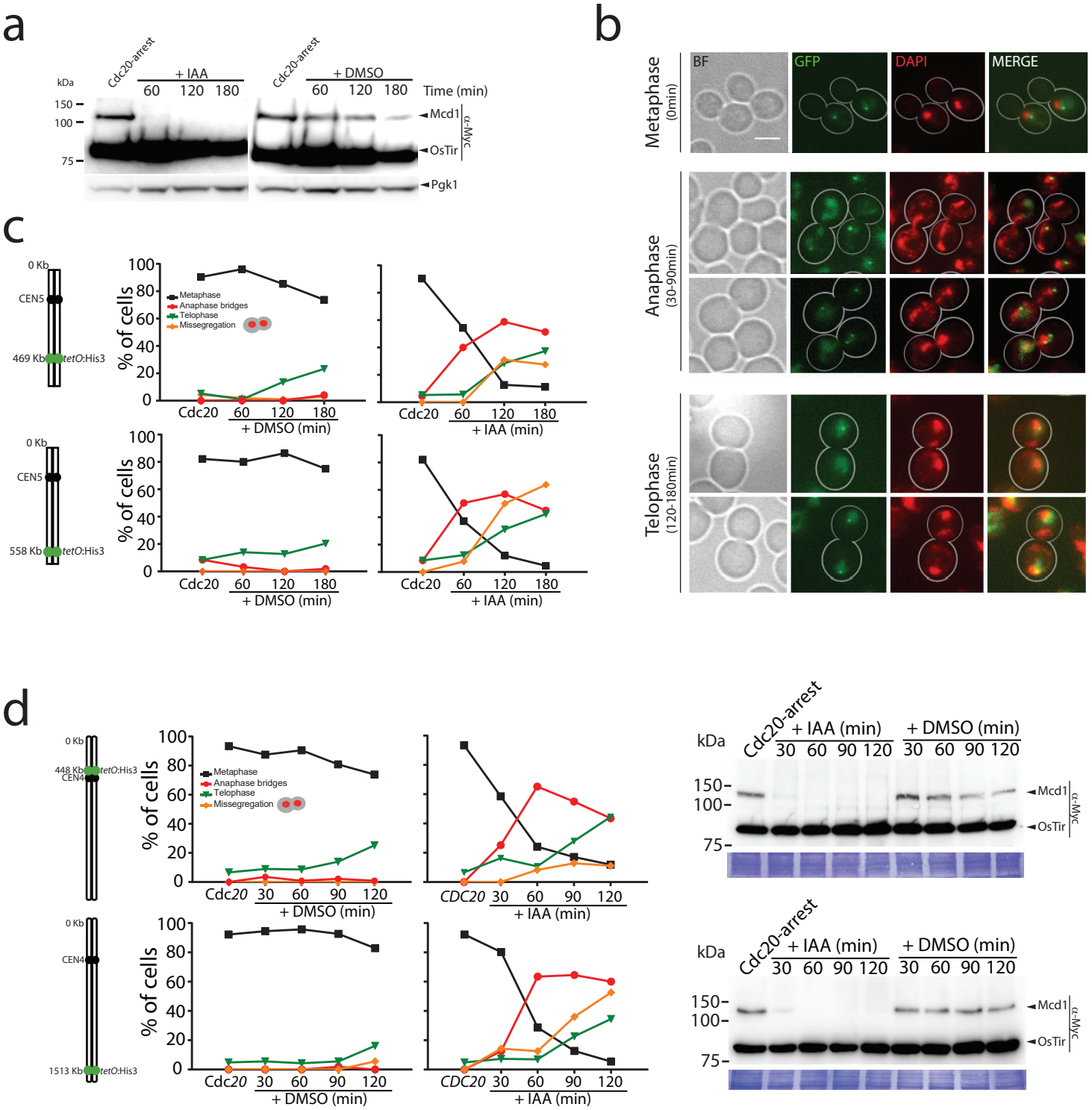
a
Cdc20-arrest
+ IAA
60 120 180
Cdc20-arrest
+ DMSO
60 120 180
Time (min)
kDa
150
100
75
Mcd1
OsTir
α-Myc
Pgk1
b
Metaphase (0min)
Anaphase (30-90min)
Telophase (120-180min)
BF
GFP
DAPI
MERGE
c
0 Kb
CEN5
469 Kb
tetO:His3
558 Kb
% of cells
Metaphase
Anaphase bridges
Telophase
Missegregation
Cdc20 60 120 180
+ DMSO (min)
+ IAA (min)
d
448 Kb
CEN4
1513 Kb
Cdc20 30 60 90 120
CDC20 30 60 90 120
+ IAA (min)
+ DMSO (min)
e
Chr. V
Chromosome V ChIP coordinates
Smc3-PK6 ChIP
Cdc20 arrest
30 min Mcd1-TEVF anaphase
60 min Mcd1-TEVF anaphase
30 min Mcd1-AID anaphase
60 min Mcd1-AID anaphase
% signal level compared to Cdc20 arrest
ChIP V loci

Figure 4

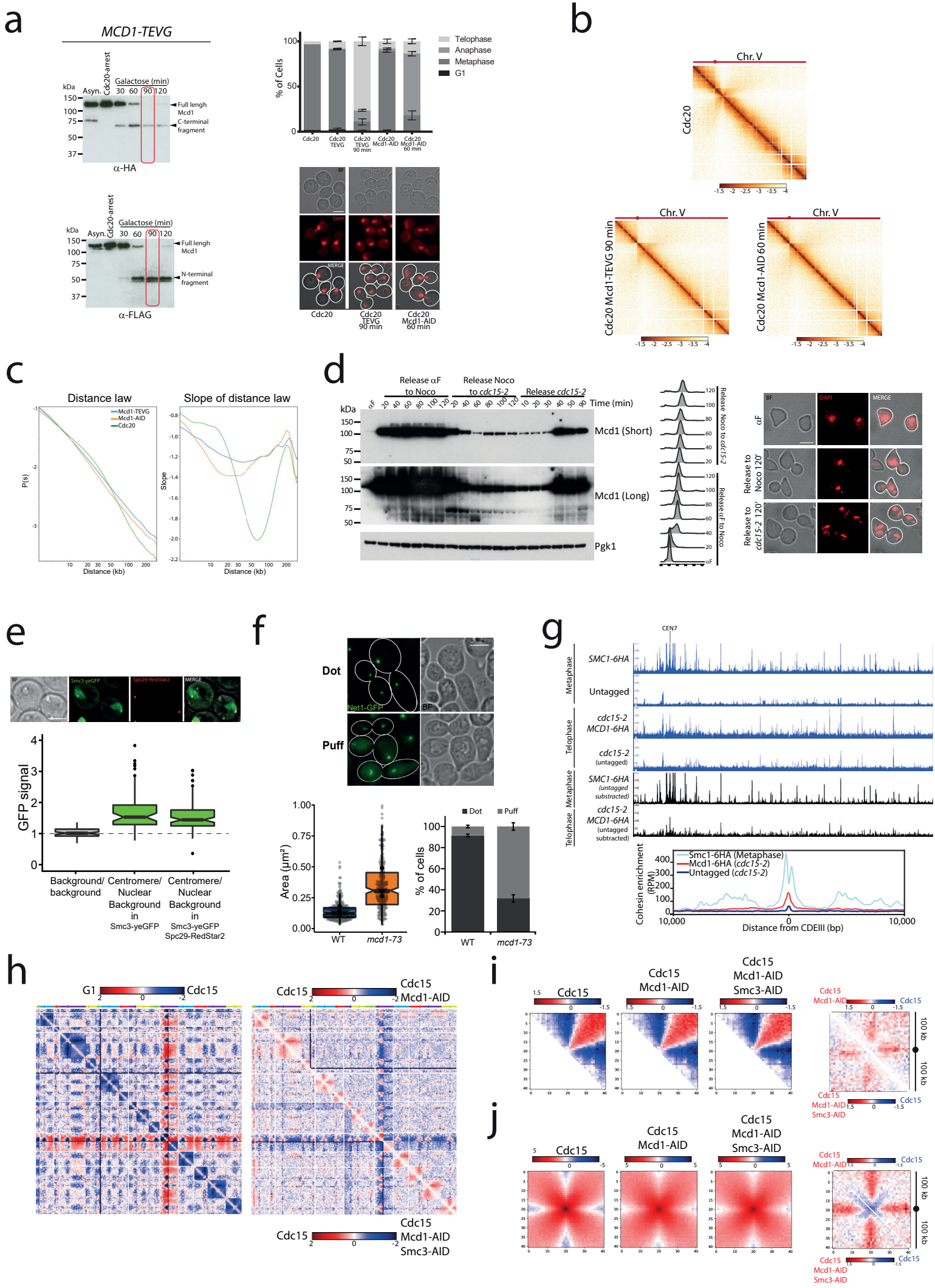
a
MCD1-TEVG
Cdc20-arrest
Galactose (min)
Asyn. 30 60 90 120
kDa
150
100
75
50
37
Full lengh Mcd1
C-terminal fragment
α-HA
N-terminal fragment
α-FLAG
% of Cells
Telophase
Anaphase
Metaphase
G1
Cdc20
Cdc20 TEVG
Cdc20 TEVG 90 min
Cdc20 Mcd1-AID
Cdc20 Mcd1-AID 60 min
BF
DAPI
MERGE
b
Chr. V
Cdc20
Cdc20 Mcd1-TEVG 90 min
Cdc20 Mcd1-AID 60 min
c
Distance law
Slope of distance law
Mcd1-TEVG
Mcd1-AID
Cdc20
P(s)
Slope
Distance (kb)
d
Release αF to Noco
Release Noco to cdc15-2
Release cdc15-2
Time (min)
Mcd1 (Short)
Mcd1 (Long)
Pgk1
Release Noco to cdc15-2
Release αF to Noco
αF
Release to Noco 120'
Release to cdc15-2 120'
e
Smc3-yeGFP
Spc29-RedStar2
GFP signal
Background/ background
Centromere/ Nuclear Background in Smc3-yeGFP
Centromere/ Nuclear Background in Smc3-yeGFP Spc29-RedStar2
f
Dot
Puff
Net1-GFP
Area (μm²)
WT
mcd1-73
% of cells
Dot
Puff
g
CEN7
Metaphase
Telophase
SMC1-6HA
Untagged
cdc15-2 MCD1-6HA
cdc15-2 (untagged)
SMC1-6HA (untagged substracted)
cdc15-2 MCD1-6HA (untagged subtracted)
Smc1-6HA (Metaphase)
Mcd1-6HA (cdc15-2)
Untagged (cdc15-2)
Cohesin enrichment (RPM)
Distance from CDEIII (bp)
h
G1
Cdc15
Cdc15
Mcd1-AID
Smc3-AID
i
Cdc15
Cdc15 Mcd1-AID
Cdc15 Mcd1-AID Smc3-AID
100 kb
j

Figure 5

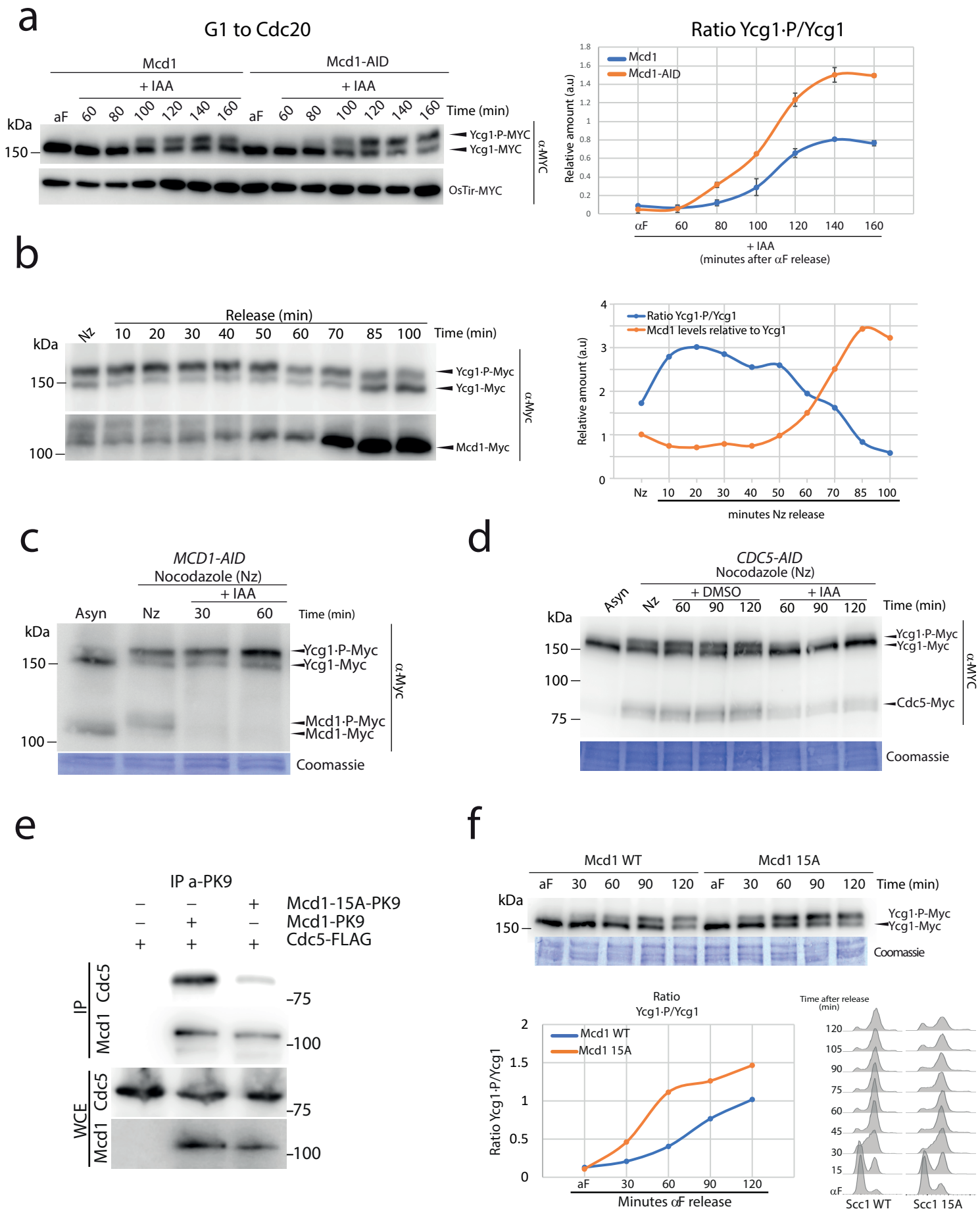
a
G1 to Cdc20
Mcd1
Mcd1-AID
+ IAA
+ IAA
aF 60 80 100 120 140 160 aF 60 80 100 120 140 160
Time (min)
kDa
150
Ycg1·P-MYC
Ycg1-MYC
OsTir-MYC
α-MYC
Ratio Ycg1·P/Ycg1
Mcd1
Mcd1-AID
Relative amount (a.u)
αF 60 80 100 120 140 160
+ IAA
(minutes after αF release)
b
Release (min)
Nz 10 20 30 40 50 60 70 85 100
Time (min)
kDa
150
100
Ycg1·P-Myc
Ycg1-Myc
Mcd1-Myc
α-Myc
Ratio Ycg1·P/Ycg1
Mcd1 levels relative to Ycg1
Relative amount (a.u)
Nz 10 20 30 40 50 60 70 85 100
minutes Nz release
c
MCD1-AID
Nocodazole (Nz)
+ IAA
Asyn Nz 30 60
Time (min)
kDa
150
100
Ycg1·P-Myc
Ycg1-Myc
Mcd1·P-Myc
Mcd1-Myc
α-Myc
Coomassie
d
CDC5-AID
Nocodazole (Nz)
Asyn Nz
+ DMSO
+ IAA
60 90 120 60 90 120
Time (min)
kDa
150
100
75
Ycg1·P-Myc
Ycg1-Myc
Cdc5-Myc
α-MYC
Coomassie
e
IP a-PK9
Mcd1-15A-PK9
Mcd1-PK9
Cdc5-FLAG
IP
Cdc5
Mcd1
WCE
Cdc5
Mcd1
75
100
75
100
f
Mcd1 WT
Mcd1 15A
aF 30 60 90 120 aF 30 60 90 120
Time (min)
kDa
150
Ycg1·P-Myc
Ycg1-Myc
Coomassie
Ratio
Ycg1·P/Ycg1
Mcd1 WT
Mcd1 15A
Ratio Ycg1·P/Ycg1
aF 30 60 90 120
Minutes αF release
Time after release (min)
120
105
90
75
60
45
30
15
αF
Scc1 WT
Scc1 15A

Figure 6

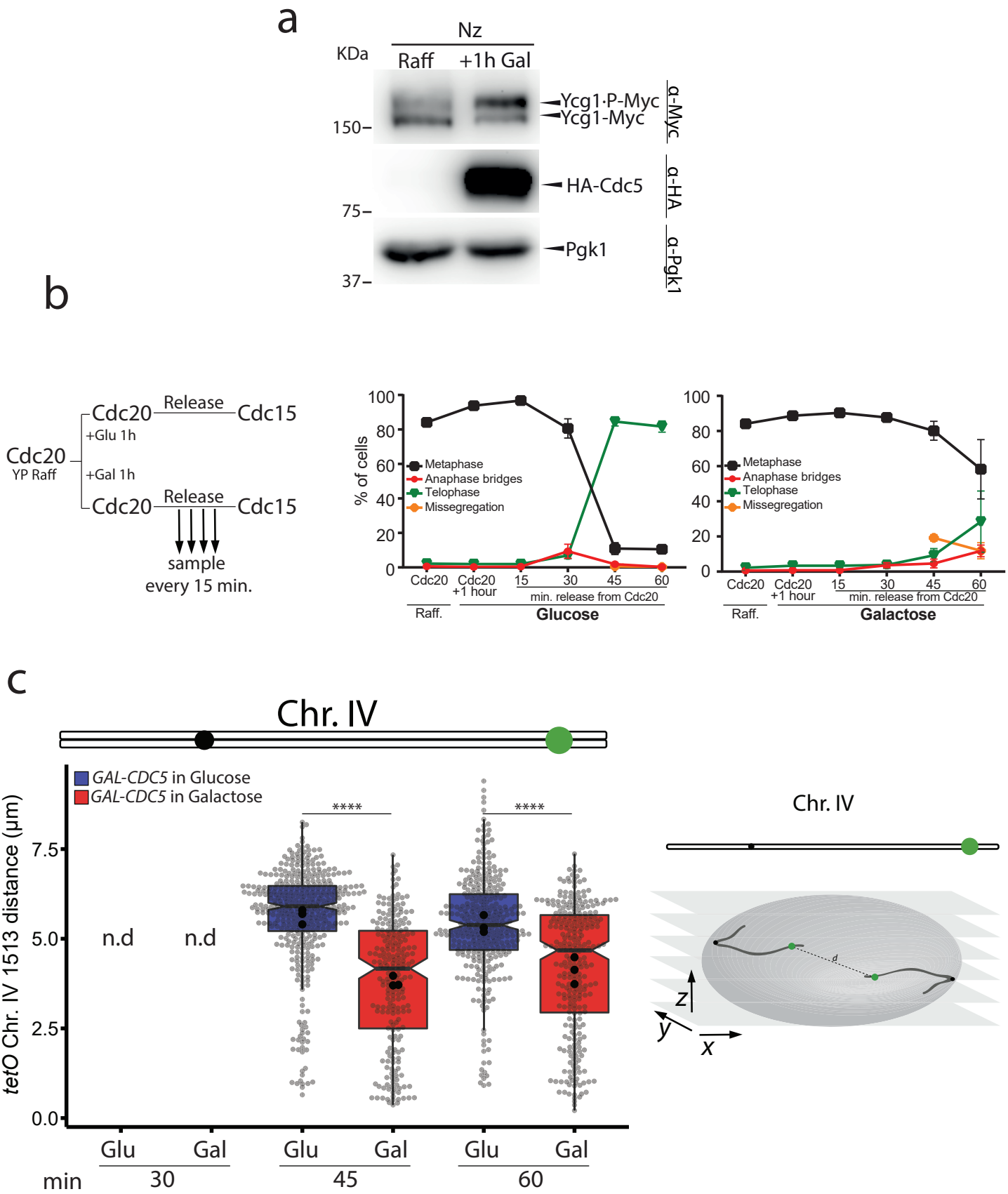
a
Nz
KDa
Raff
+1h Gal
150–
75–
37–
Ycg1·P-Myc
Ycg1-Myc
HA-Cdc5
Pgk1
α-Myc
α-HA
α-Pgk1
b
Cdc20
YP Raff
Cdc20
Release
Cdc15
+Glu 1h
+Gal 1h
Cdc20
Release
Cdc15
sample
every 15 min.
% of cells
Metaphase
Anaphase bridges
Telophase
Missegregation
Cdc20
Cdc20 +1 hour
15
30
45
60
min. release from Cdc20
Raff.
Glucose
Galactose
c
Chr. IV
GAL-CDC5 in Glucose
GAL-CDC5 in Galactose
tetO Chr. IV 1513 distance (µm)
7.5
5.0
2.5
0.0
n.d
n.d
****
****
Glu
Gal
Glu
Gal
Glu
Gal
min
30
45
60
Chr. IV
d
z
y
x

Figure 7

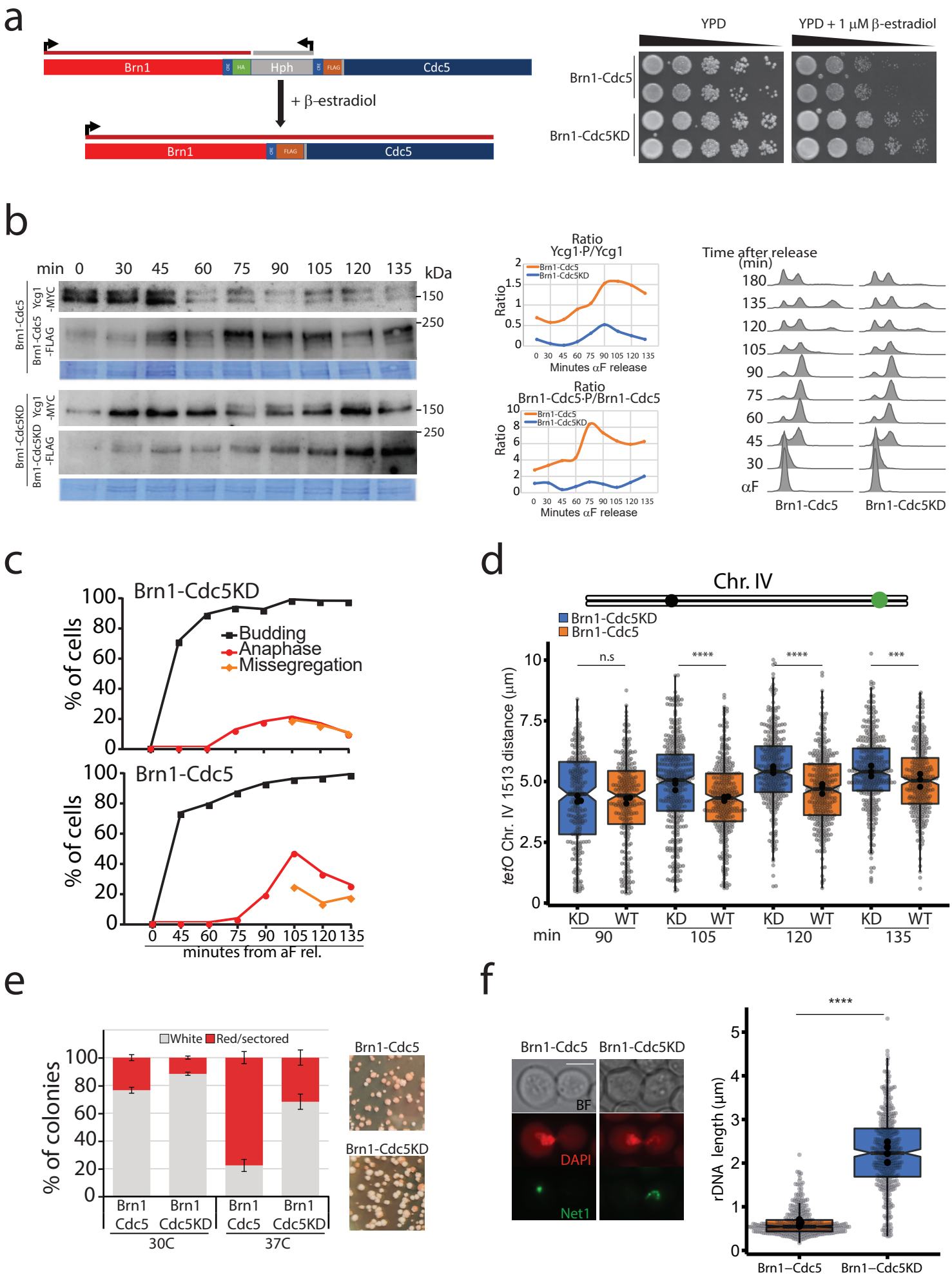
a
Brn1
Hph
Cdc5
+ β-estradiol
YPD
YPD + 1 μM β-estradiol
Brn1-Cdc5
Brn1-Cdc5KD
b
min 0 30 45 60 75 90 105 120 135
kDa
Brn1-Cdc5
Brn1-Cdc5KD
Ycg1 -MYC
Brn1-Cdc5 -FLAG
Brn1-Cdc5KD -FLAG
150
250
Ratio Ycg1-P/Ycg1
Ratio Brn1-Cdc5-P/Brn1-Cdc5
Minutes αF release
Time after release (min)
αF
c
Brn1-Cdc5KD
Brn1-Cdc5
% of cells
Budding
Anaphase
Missegregation
minutes from aF rel.
d
Chr. IV
Brn1-Cdc5KD
Brn1-Cdc5
tetO Chr. IV 1513 distance (μm)
n.s
****
***
KD WT KD WT KD WT KD WT
min 90 105 120 135
e
White
Red/sectored
% of colonies
Brn1 Cdc5
Brn1 Cdc5KD
30C
37C
f
BF
DAPI
Net1
rDNA length (μm)
Brn1–Cdc5
Brn1–Cdc5KD

Figure 8

a

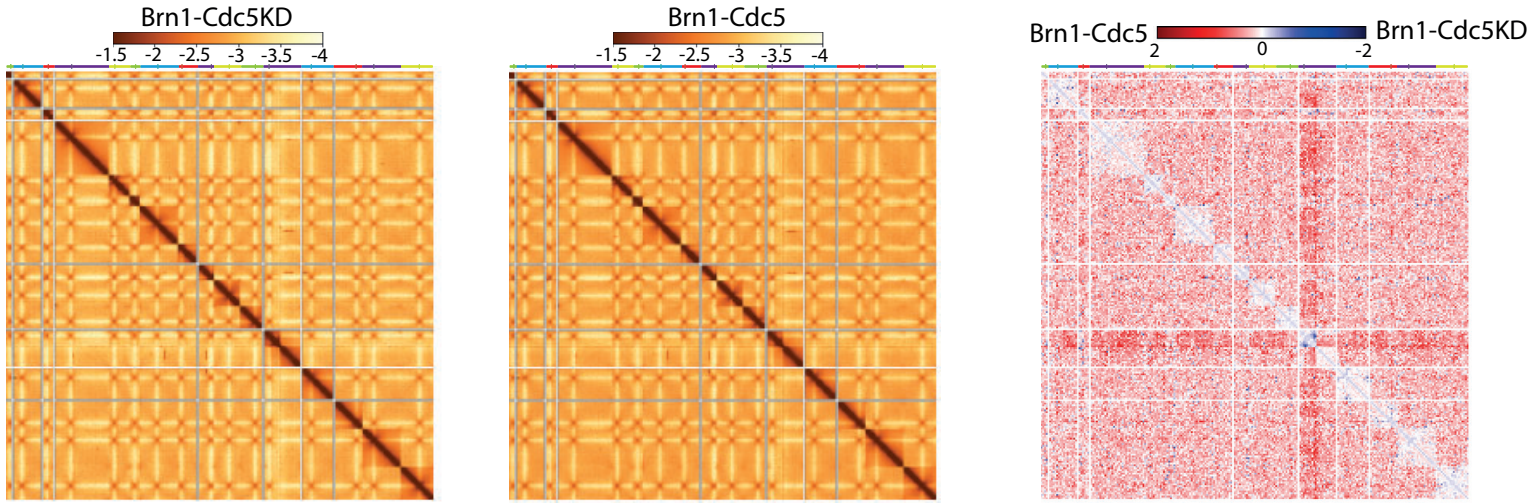

b

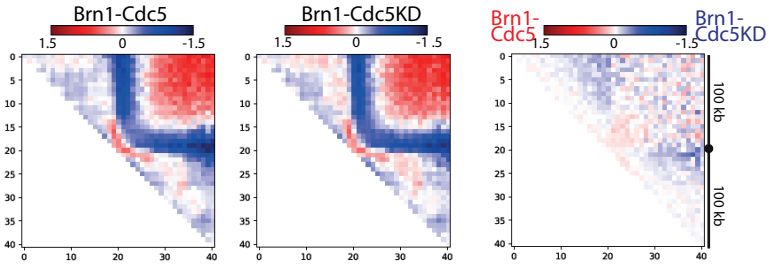

c

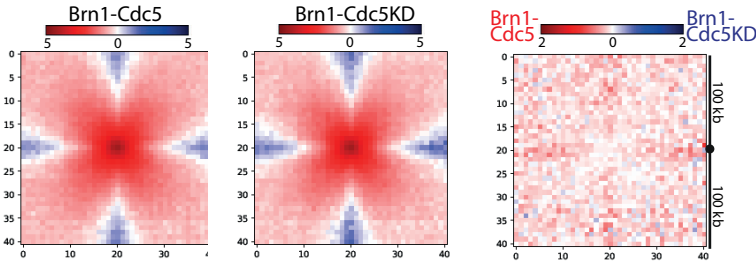

d

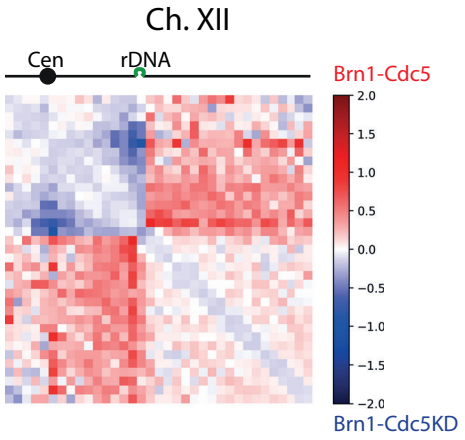

e

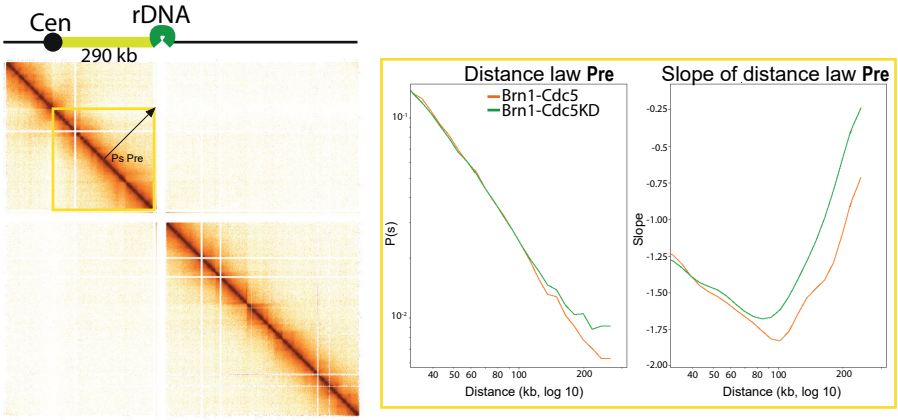

f

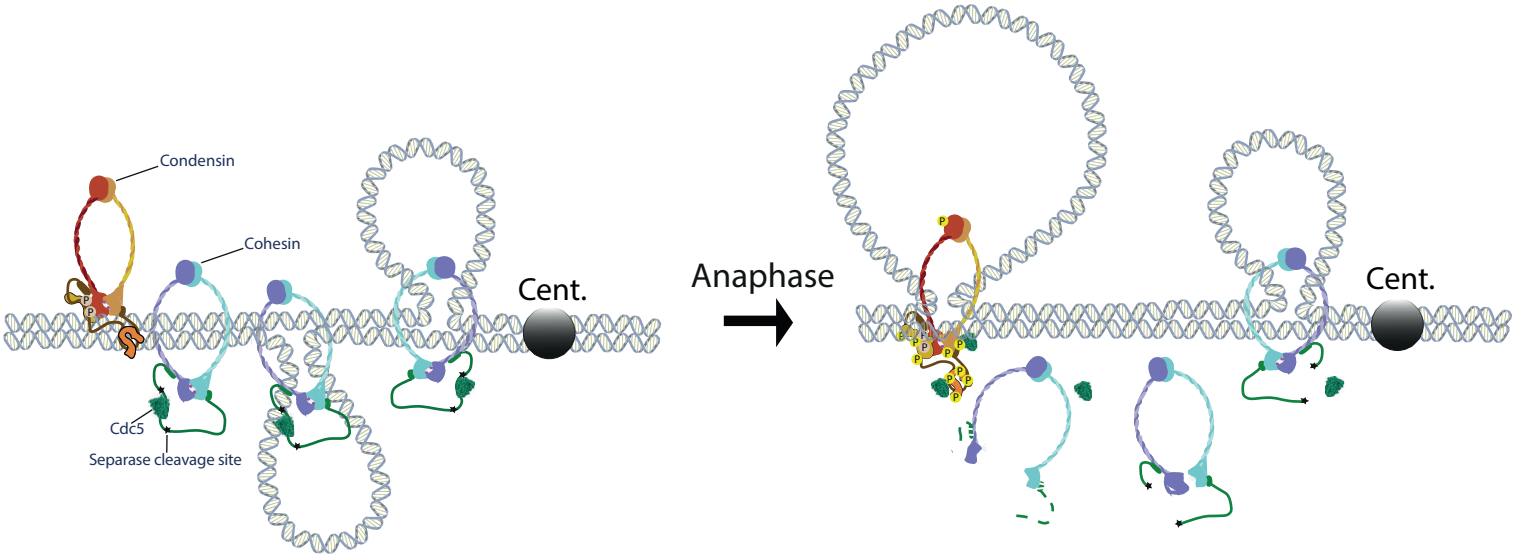

Supp. Figure 1

a

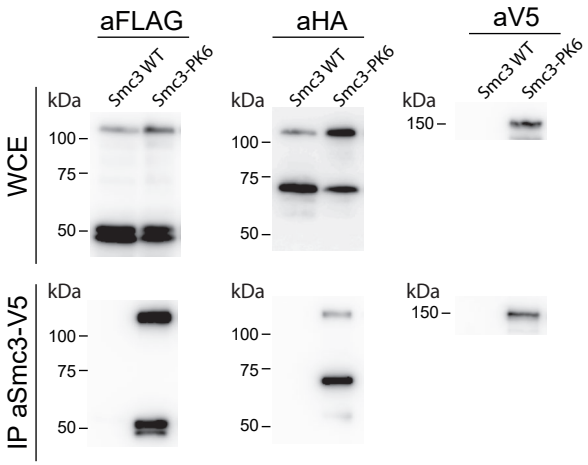

b

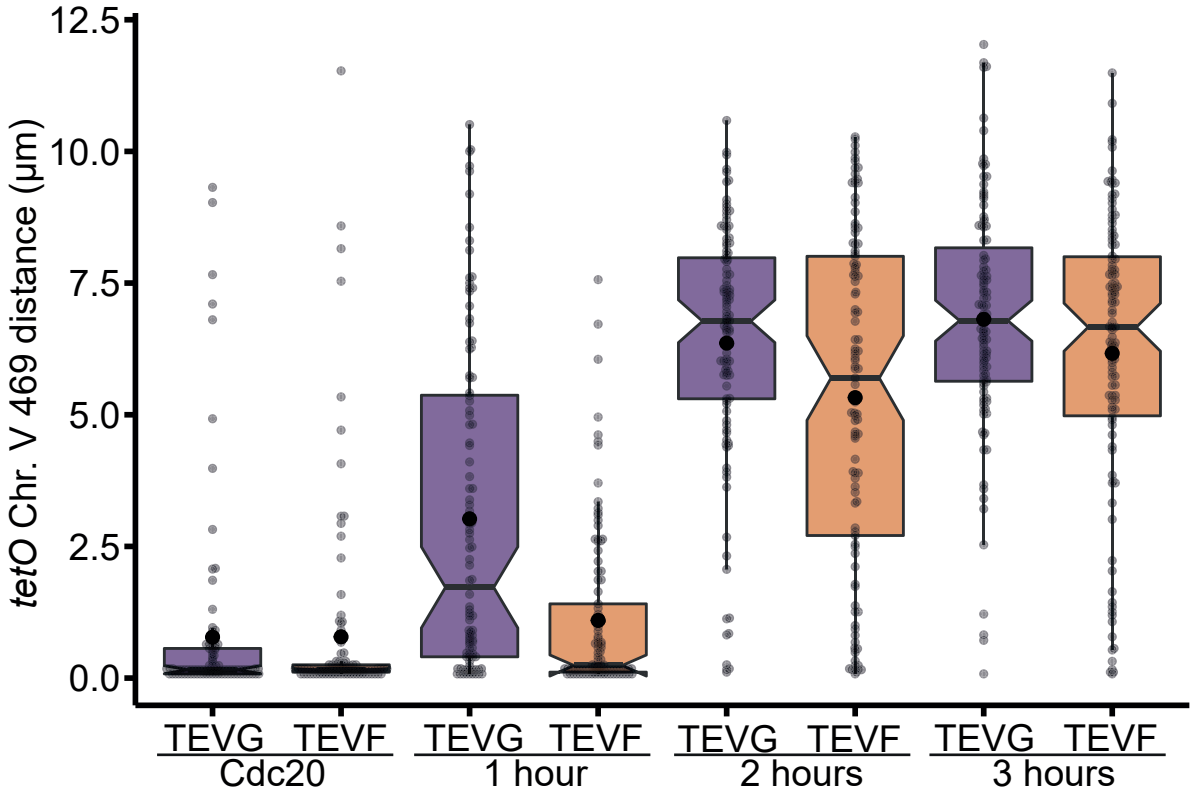

Supp. Figure 2

a

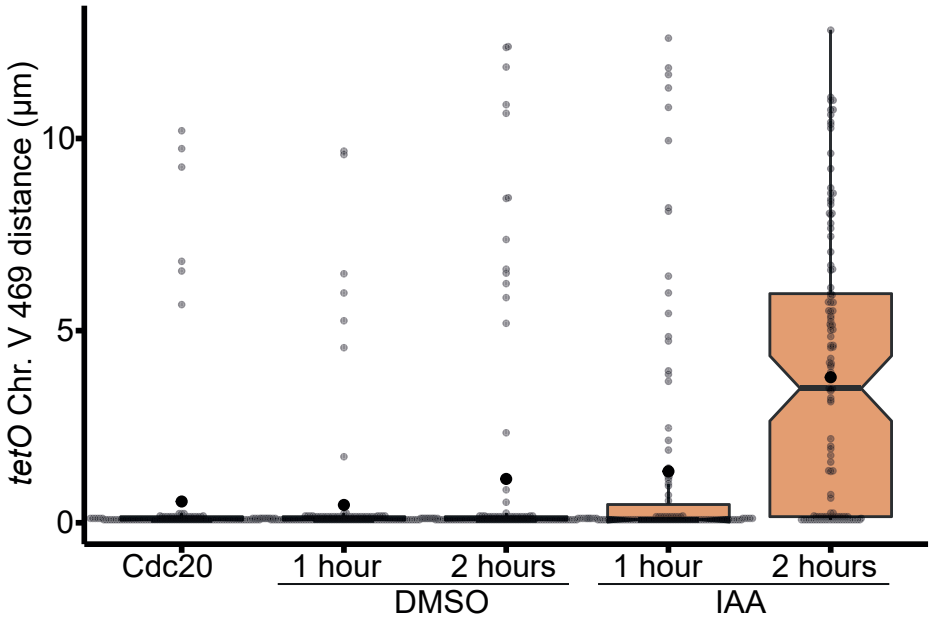

b

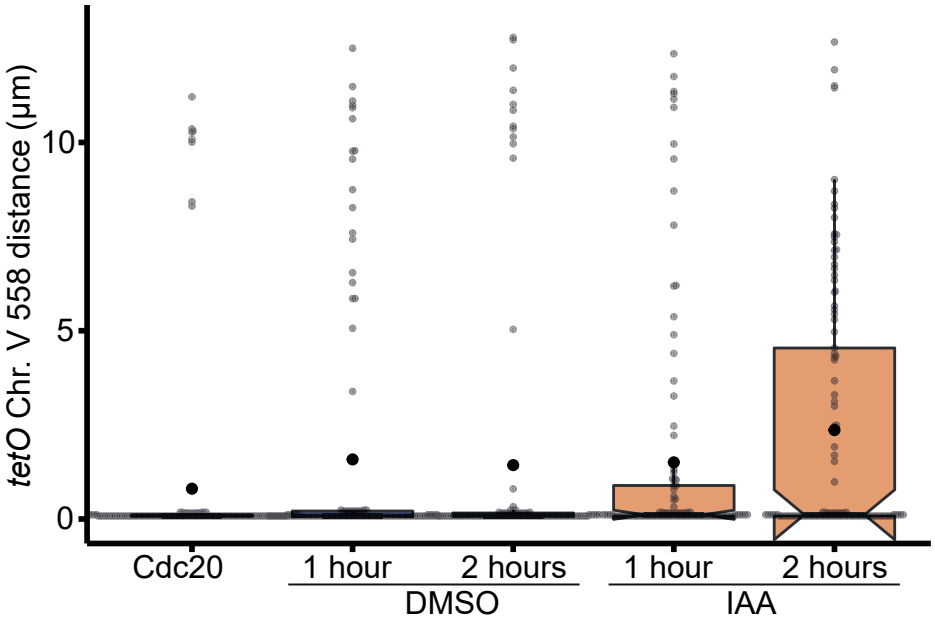

Supp. Figure 3

a

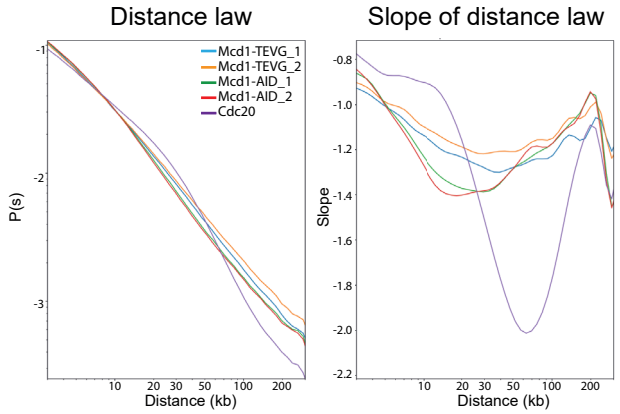

b

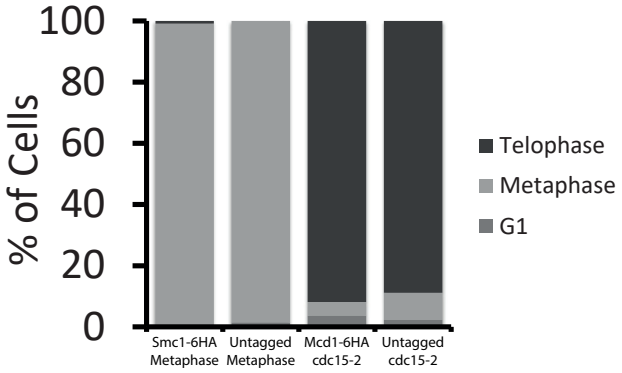

c

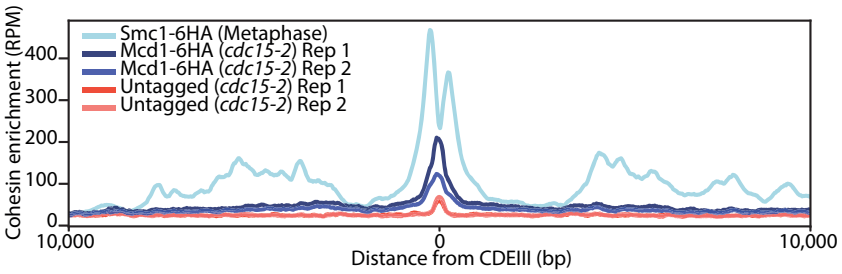

d

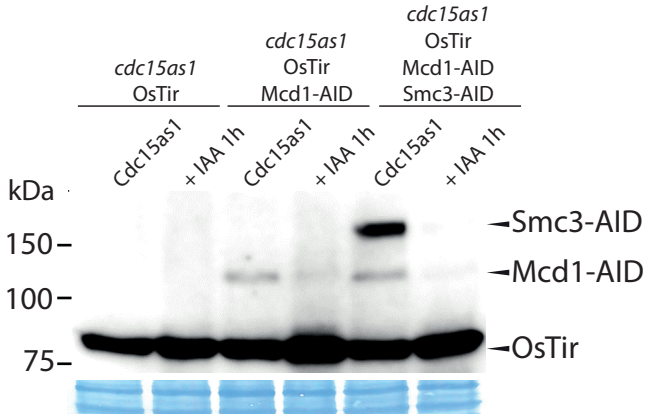

e

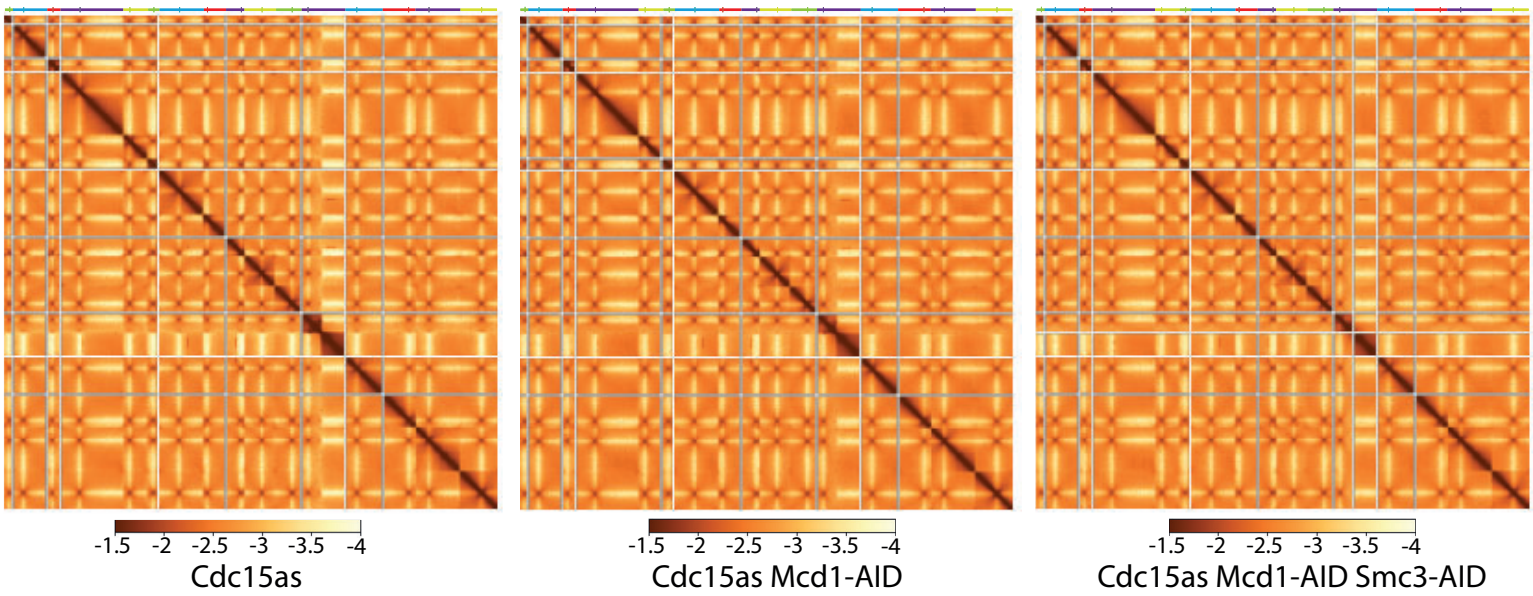

Supp. Figure 4

a

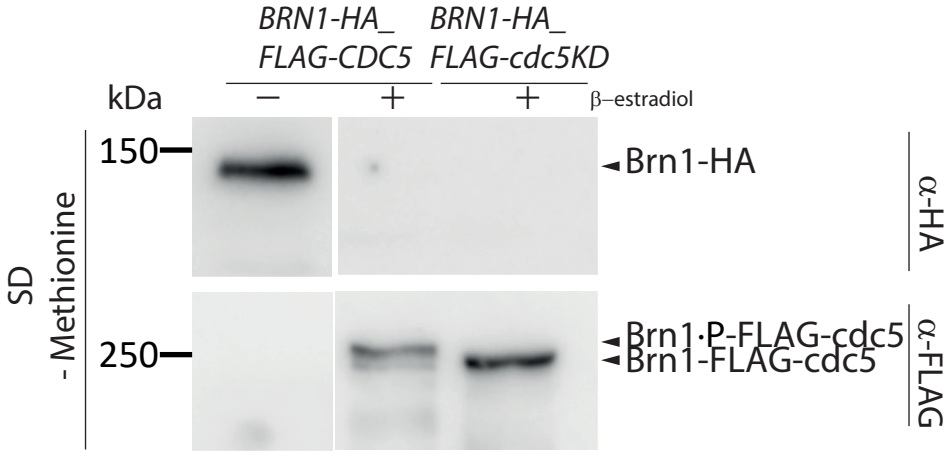

Supp. Figure 5
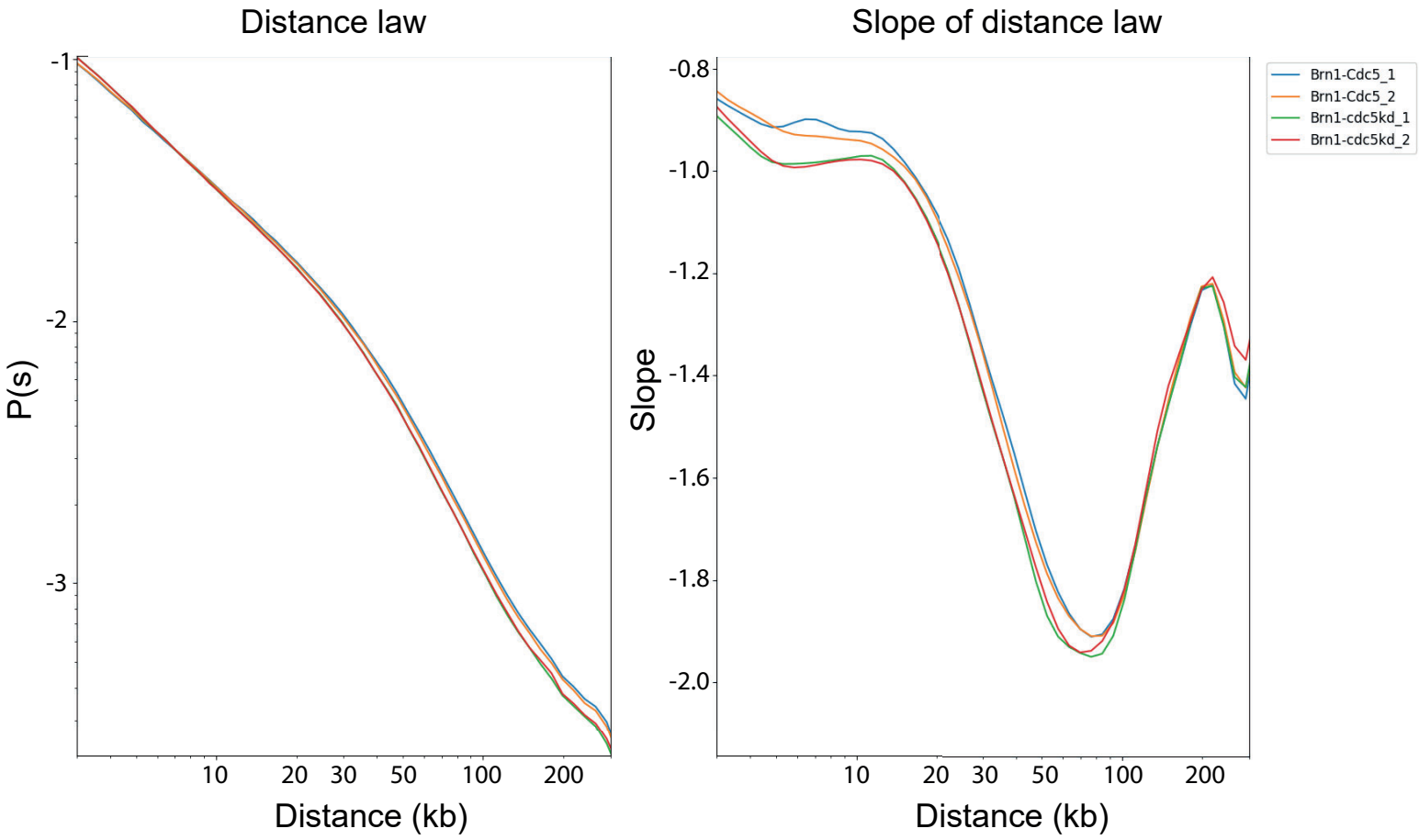
a